Nanoscale Advances

ROYAL SOCIETY OF CHEMISTRY

PAPER

View Article Online
View Journal | View Issue

Cite this: *Nanoscale Adv.*, 2025, **7**, 2988

Evaluation of the antimicrobial activity of chitosan- and curcumin-capped copper oxide nanostructures against multi-drug-resistant microorganisms†

Noura El-Kattan,[a] Mostafa A. Ibrahim,[b] Ahmed N. Emam, *[cd] Khaled Metwally, [e] Fady Sayed Youssef,[f] Nourelhuda Ahmed Nassar[g] and Ahmed S. Mansour[hi]

The emergence of multi-drug-resistant microorganisms presents a serious threat to infection control, for which new antimicrobial strategies are urgently needed. Herein, the antimicrobial activities of copper oxide nanoparticles capped with curcumin (Cur-CuO NPs) and copper oxide nanoparticles capped with chitosan (CS-CuO NPs) were investigated. They were prepared *via* the co-precipitation method. A total of 180 clinical ICU patients were found to have 70% Gram-negative and 30% Gram-positive isolates. Antimicrobial susceptibility testing indicated resistance of these isolates to 14 among the 21 tested antibiotics. Physicochemical properties of the curcumin-capped (Cur-CuO NPs) and chitosan-capped (CS-CuO NPs) copper oxide nanoparticles were identified using UV-vis spectroscopy, transmission electron microscopy (TEM), dynamic light scattering (DLS), zeta-potential (ζ), and Fourier transform infrared (FT-IR) spectroscopy. Cur-CuO- and CS-CuO-NPs exhibited potent antimicrobial efficacy, wherein CS-CuO NPs were found to possess a lower minimum inhibitory concentration (MIC) (3.9–15.6 μg mL^{-1}) than Cur-CuO NPs (14.5–31.2 μg mL^{-1}). Biocompatibility assay showed that Cur-CuO NPs were safer with an IC_{50} dose of 74.17 μg mL^{-1} than CS-CuO NPs with an IC_{50} dose of 41.01 μg mL^{-1}. Results revealed that the Cur-CuO- and CS-CuO-NPs have the potential to be safely used as effective antimicrobial agents in clinical applications at low concentrations (6.25–12.5 μg mL^{-1}).

Received 18th November 2024
Accepted 18th March 2025

DOI: 10.1039/d4na00955j

rsc.li/nanoscale-advances

1. Introduction

Nosocomial infections are among the most significant global health care problems and have an unfavorable impact on clinical outcomes.[1,2] The rise of multidrug-resistant bacteria poses a critical challenge to medical treatment, as these organisms can withstand multiple antimicrobial interventions, severely limiting therapeutic options.[3] The pathogeny of antibiotic-resistant genes in diverse bacterial species has emerged owing to the misuse of antibiotics. According to researchers, antimicrobial nano-formulation is a promising avenue of future research owing to the significant antimicrobial activities exhibited by nanomaterials.[4] Nanoparticles with a size of less than 100 nm are increasingly replacing the application of traditional antibiotics in medicine. Nanobiotechnology in the future is expected to bring the development of new antibacterial agents *via* the production of important size- and form-specific metal oxide nanoparticles. Metal oxide nanoparticles are of great interest owing to their functionalities in electric-, electrochemical-, paint/ink materials, catalysis, and magnetism.[5–7]

Copper oxide nanoparticles and other metal oxide nanoparticles are now the focus of research because of their antibacterial and biocidal properties, which are employed in many biological applications.[5] Silver, zinc oxide, titanium oxide, copper oxide, and iron oxide nanoparticles are the most widely used in antimicrobial research. However, silver is expensive, and thus, there is a need for inexpensive materials that can yield

[a]*Department of Microbiology, Research Institute of Medical Entomology, General Organization for Teaching Hospitals and Institutes, Giza, Egypt*
[b]*Production and R&D Unit, NanoFab Technology Company, 6th October City, Giza, Egypt*
[c]*Refractories, Ceramics and Building Materials Department, Advanced Materials Technology & Mineral Resources Research Institute, National Research Centre (NRC), El Bohouth St., Dokki, 12622 Cairo, Egypt. E-mail: ahmed.gsc.ndp@gmail.com; an.emam@nrc.sci.eg*
[d]*Nanomedicine & Tissue Engineering Research Lab, Medical Research Centre of Excellence, National Research Centre (NRC), El Bohouth St., Dokki, 12622 Cairo, Egypt*
[e]*Genetics Department, Faculty of Agriculture, Ain Shams University, P.O. Box 68, Hadayek Shoubra, 11241, Cairo, Egypt*
[f]*Department of Pharmacology Faculty of Veterinary Medicine, Cairo University, 12211 Giza, Egypt*
[g]*Clinical Pathology Department, Al-Sahel Teaching Hospital, Cairo, Egypt*
[h]*Department of Laser Applications in Meteorology, Chemistry and Agriculture, National Institute of Laser Enhanced Sciences (NILES), Cairo University, Cairo, Egypt*
[i]*Faculty of Postgraduate Studies for Nanotechnology, Cairo University, Zayed City, Giza, Egypt*

† Electronic supplementary information (ESI) available. See DOI: https://doi.org/10.1039/d4na00955j

equivalent efficacy. Copper presents antibacterial possibilities in making antimicrobial textiles. Antibacterial action can cause ROS generation, destruction of the cell membrane through electrostatic interactions, disruption in metal/metal ion homeostasis, and dysfunction of proteins and enzymes.[8] The antibacterial activities of copper and copper oxide nanoparticles are well documented and are said to work against bacteria by puncturing their cell membranes and impairing their vital enzymes. Nevertheless, in the case of Gram-positive and Gram-negative bacteria, which are generally negatively charged, Gram-positive bacteria with a thick peptidoglycan cover will be influenced more than Gram-negative bacteria with a sophisticated structure on metal uptake.[9,10] Electrostatic interactions will attract the positively charged nanoparticles and disrupt the cell wall with increased permeability. The nanoparticles release the metal ions from their extracellular environment, inducing a biological response and generation of reactive oxygen species (ROS) using the above-mentioned pathways. Metal ions will bind to the cellular constituents, thereby disrupting cell activities and creating very strong coordination bonds with organic and biomolecular fragments.[11,12]

CuO NPs possess better antibacterial properties than silver NPs.[13] Throughout history, copper has been recognized for its powerful antimicrobial properties, demonstrating the ability to eliminate up to 99.9% of microorganisms through its metal oxide interactions. Copper/copper oxide NPs exhibit extensive antimicrobial action against Gram-positive as well as Gram-negative bacteria, thereby eradicating these pathogens, which are responsible for hospital-acquired infections.[14] The antibacterial effect by CuO NPs is determined regarding bacterial cell properties, which is especially significant in terms of cell wall structure and Gram character. CuO NPs destroyed 100% of Gram-negative *E. coli* at concentrations greater than 9.5%, while the same concentration was less effective against Gram-positive *S. aureus*.[15,16] Antibacterial activity is affected by particle size and surface properties, where smaller particles have more antibacterial power because of their higher surface area.[17,18] Although limited studies have been done on CuO NPs, they present good potential bactericidal activity for a variety of infectious organisms including *E. coli*, *B. subtilis*, *V. cholera*, *P. aeruginosa*, *S. typhus*, and *S. aureus*.[19–21]

Turmeric curcumin extract (*Curcuma longa* Linns/*Curcuma domestica* Valeton) can be used as a biocompatible reducing and capping agent during the synthesis of nanoparticles. This compound has been used as a spice, food color,[22] and Chinese medicine for thousands of years and possesses multiple therapeutic activities such as antioxidant, anti-inflammatory, antiseptic, and anticancer activities.[23–28] FDA has approved the safety of curcumin in a dose of up to 12 g per day.[29] Similar to antibiotics, curcumin possesses more than one way of killing bacteria including causing membrane damage, production of reactive oxygen species (ROS), inhibition of efflux pumps, and inhibition of cell division. The abundant hydroxyl groups in the phenolic molecules in curcumin interact with the bacterial cell membrane in a specific manner. This results in the loss of permeability and alteration in fatty acid and phospholipid profiles, hence inhibiting energy metabolism and *de novo* synthesis of its genetic material. Curcumin has been shown experimentally to cause high dose rumpling of Gram-positive (*S. aureus* and *Enterococcus faecalis*) and Gram-negative (*E. coli* and *Pseudomonas aeruginosa*) bacteria membranes, cause apoptosis of bacterial cells, and markedly suppresses the efflux pump resistance mechanisms of bacteria such as *P. aeruginosa* and *S. aureus*.[30,31]

Chitosan is a shellfish and crustacean-derived polysaccharide from chitin.[32] It can be used in tissue engineering for treating hypertension and high cholesterol, and wound healing due to its antioxidant and antibacterial properties.[33] Chitosan possesses an advantageous property of compatibility with metals, metal oxide nanoparticles, and polymers. Its antimicrobial effect is through the disruption of microbial cell membranes through electrostatic interaction between its positively charged amino groups and the negatively charged cell surface components;[32] inhibition of nutrient transfer in Gram-negative bacteria (high-molecular-weight chitosan); and inhibition of DNA/RNA and protein synthesis (low-molecular-weight chitosan).[34,35] Chitosan also serves as a template in the synthesis of metal oxide nanoparticles, which can alter the surface properties of the resulting particles.[36–38]

To the best of our knowledge, the antimicrobial efficacy of chitosan-capped CuO NPs and curcumin-capped CuO NPs against multi-drug-resistant microbes has yet to be studied except in a few reports.[39–45] The present study aimed to evaluate the antibacterial activity of green-synthesized copper oxide nanoparticles (CuO NPs) in the presence of curcumin against the multi-drug-resistant (MDR) bacteria, which existed in the turmeric ethanolic extract and chitosan extracts. In addition, efficient hybrid nanocomposites were developed based on the formation of chitosan-capped CuO (CS-CuO NPs) and curcumin-capped CuO (Cur-CuO NPs) nanoparticles. The morphological, optical, surface and colloidal properties of the as-prepared nanoparticles were investigated using TEM, UV-vis absorption spectroscopy, FT-IR, DLS and zeta-potential measurements. In addition, the antimicrobial activity of both CS-CuO and Cur-CuO NPs was tested against the most popular MDR microbes in Egyptian hospitals, especially in the intensive care unit (ICU). Our results revealed that the chitosan-capped CuO NPs have higher antimicrobial efficacy with a lower minimum inhibition concentration (MIC) than previously reported values in the literature. Also, the curcumin-capped CuO NPs exhibited significant antimicrobial activity against MDR microbes with a lower MIC than that reported in the previous study by Varaprasad *et al.*[45] Finally, Cur-CuO NPs showed remarkable biocompatibility, which was higher than that previously reported by Varaprasad *et al.*[45] All these results indicate that Cur-CuO and CS-CuO NPs can be used as active ingredients in antimicrobial coating paint applications.

2. Experimental

2.1. Materials

Copper(II) sulfate pentahydrate LR ($CuSO_4 \cdot 5H_2O$, 98.5%) was purchased from SD-Fine Chem Limited. Ethanol absolute (C_2H_5OH, EtOH 95%) was obtained from Central Drug House (P)

LTD, chitosan medium molecular weight (CS M. wt. 200 000–350,000, 99%) was from Alpha Chemika, and turmeric powder (*Curcuma longa* Linns, "synonym; *Curcuma domestica* Valeton, Zingiberaceae") was obtained from the local spice market as an imported product from India by Aava Ayurveda Private Limited, Ludhiana, India. Pure curcumin as the standard was purchased from Herbal House Centers, (Egypt – Lot No. HHC092021). Mueller–Hinton Agar (Oxoid Limited, Cat. No. CM0337), antibiotics including amikacin, amoxicillin/clavulanic acid, tigecycline, cefepime, cefotaxime, ceftazidime, cefaclor, ciprofloxacin, gentamicin, imipenem, meropenem, levofloxacin, tetracycline, tobramycin, cefazolin, and cefoxitin were purchased from Oxoid Limited. SRPMI-1640 medium, MTT, and DMSO were obtained from Sigma Co., St. Louis, USA, and fetal bovine serum was from GIBCO, UK.

2.2. Methods

2.2.1. Extraction of curcumin from *Curcuma longa* Linns powder. The extraction of curcumin from turmeric (*i.e.*, *Curcuma longa* Linns (*C. longa*)) powder was carried out in the current study as reported in our previous study.[4] Typically, 100 g of turmeric powder from *C. longa* rhizomes was added to 1 L of absolute ethanol under vigorous stirring and refluxed at 60 °C for 24 h. Then, the mixture was filtered with Whatman filter paper. The extracted curcumin yield was calculated by drying the residue from the extraction at room temperature, and then weighing it to determine the extracted curcumin yield. The extracted curcumin from the turmeric (*i.e.*, *C. longa*) ethanolic extract was validated against pure curcumin (Herbal House Center, Egypt – Lot No. HHC092021) using two spectroscopic techniques, UV-vis absorption/fluorescence spectroscopy, thin-layer chromatography (TLC),[4] and GC-MS chromatography.

2.2.2. Identification and validation of the ethanolic extract of turmeric (*Curcuma longa* Linn) powder *vs.* pure curcumin. The ethanolic extract of *Curcuma longa* Linns plant powder and pure curcumin samples were extracted, dried, and resuspended in 50 μL of bis(trimethylsilyl)trifluoroacetamide (BSTFA) + trimethylchlorosilane (TMCS) 99 : 1 silylation reagent and 50 μL pyridine to derivatize the functional groups in the samples to trimethylsilyl groups (abbreviated TMS) before GC measurement. Gas chromatography-mass spectrometry analysis (GC-MS). The Central Laboratories Network, National Research Centre, Cairo, Egypt, used an Agilent Technologies GC-MS system with a gas chromatograph (7890B) and a mass spectrometer detector (5977A). The GC had an HP-5MS column (30 mm × 0.25 mm internal diameter, 0.25 μm film thickness). Analyses were conducted using hydrogen as the carrier gas at a flow rate of 2.0 mL min^{-1}, splitless injection volume of 2 μL, and the following temperature program: 50 °C for 5 min; increase at 5 °C min^{-1} to 100 °C and hold for 0 min; then increase at 10 °C min^{-1} to 320 °C and hold for 10 min. The injector and detector were kept at 280 °C and 320 °C, respectively. Mass spectra were acquired using electron ionization (EI) at 70 eV, in the spectral range of m/z 25–700 and a solvent delay of 6 min. The temperature of the source was 230 °C, while that of the quad was 150 °C. Various constituents were discovered by comparing the spectrum fragmentation pattern to that in the Wiley and NIST databases.

2.2.3. Fabrication of curcumin capped-copper oxide nanoparticles (Cur-CuO NPs). Curcumin-capped copper oxide nanoparticles (Cur-CuO NPs) were synthesized *via* the co-precipitation method using the ethanolic extract of turmeric (*i.e.*, *Curcuma longa* Linns) powder, as reported previously, with slight modification.[46–48] A 50 mL aqueous solution of 0.1 M copper(II) sulfate pentahydrate ($CuSO_4 \cdot 5H_2O$) was applied dropwise to 200 mL extract and heated at 60 °C for 2 h on a magnetic stirrer. The reaction color changed from blue to a dark-brownish-yellow solution, indicating the formation of Cur-CuO NPs. Then, the reaction mixture was cooled to room temperature. This brownish-yellow solution was purified through centrifugation at 10 000 rpm for 15 min (SIGMA, Germany). The resulting pellet was dried in an oven at 100 °C. The collected precipitate was ground into a fine powder, followed by calcination for 2 h at 500 °C to get brownish-black powder.

2.2.4. Fabrication of chitosan capped-copper oxide nanoparticles (CS-CuO NPs). Chitosan-capped copper oxide nanoparticles (CS-CuO NPs) were synthesized *via* the co-precipitation method using an aqueous chitosan solution, as reported previously, with a few modifications.[37,40,49] Typically, about 2 g of medium molecular weight chitosan (CS) was dissolved in an aqueous 1% acetic acid solution at 60 °C under vigorous stirring until a clear off-white solution was obtained, indicating indicates that CS was completely dissolved. Then, 0.1 M of $CuSO_4 \cdot 5H_2O$ aqueous solution was applied dropwise to the CS solution under vigorous stirring at 70 °C for 3 h. The reaction mixture color changed from blue to green, and ultimately greenish black.

2.3. Characterization

The photophysical properties, including the UV-vis absorption spectra to provide insights into the electronic transitions, of the as-green synthesized curcumin (Cur-CuO) and chitosan-capped (CS-CuO) copper oxide nanoparticles were investigated using a TG-80 double beam spectrophotometer. The absorption spectra were recorded in the range of 200 to 900 nm, with an increment and wavelength step of about 0.2 and 5 nm, respectively.

Transmission electron microscopy (TEM) JEOL, model JEM 2100F, was used to visualize the morphological properties of the obtained Cur-CuO and CS-CuO NPs at an operating voltage of 160 kV. Also, to confirm the elemental composition and presence of copper and oxygen in the nanoparticles, ensuring the successful synthesis of copper oxide nanoparticles, elemental X-ray (EDX) analysis was carried out on a TESCAN VEGA II SBU scanning electron microscope at an operating voltage in the range of 200 V to 30 kV.

Crystallographic structure was investigated by X-ray diffraction (XRD) measurements using a Bruker D8 advanced X-ray powder diffractometer operating with a Cu target with $K\alpha1 = 1.54060$ Å, $K\alpha2 = 1.5444$ Å, in the 2θ range of 10° to 50° at a step of 0.02°.

The critical information about the size distribution, surface charge (*i.e.* zeta potential), and colloidal stability for the as-

prepared curcumin and chitosan-capped CuO NPs was measured using a Malvern Zetasizer Nano ZS Nano instrument with an He/Ne laser (*i.e.*, $\lambda = 633$ nm) at an angle of 173° collecting backscatter optics.

Furthermore, FT-IR was used to identify the functional groups present in the synthesized curcumin and chitosan-capped CuO NPs and investigate the potential interactions among curcumin, chitosan, and copper oxide. FT-IR spectra were recorded in the range of 400 to 4000 cm^{-1} using a JASCO 6700 Fourier transform infrared spectrometer (FT-IR).

2.4. Microbiological investigation

2.4.1. Clinical sample collection. One hundred eighty clinical specimens, including blood, sputum, wound, and urine, were taken from patients with complaints of different infections, from both sexes and ages ranging from 28–86 years, admitted to the intensive care unit (ICU) in El-Sahel Teaching Hospital, the General Organization for Teaching Hospitals and Institutes (GOTHI), Cairo, Egypt. The different specimens were collected from patients diagnosed with infection based on clinical signs and immediately transported to the microbiology laboratory for further investigations. The clinical and laboratory data of each patient were obtained and registered, as shown in Table 1.

2.4.2. Isolation and identification of microbial isolates. Cultures were processed using standard microbiological examination.[50] Following the isolation, microbial isolates were identified using the conventional VITEK 2 compact 15-system bioMerieux.

2.4.3. Antibiotics screening test. The antimicrobial susceptibility test was performed for all bacterial isolates using the standard Kirby–Bauer disk diffusion method.[51,52] The concentration of antibiotics for disc diffusion testing for both Gram-positive and Gram-negative isolates was as follows: amikacin (30 μg), amoxycillin/clavulanic acid (30 μg), ampicillin/sulbactam (30 μg), tigecycline (15 μg), cefepime (30 μg), cefotaxime (10 μg), ceftazidime (30 μg), ciprofloxacin (5 μg), gentamicin (10 μg), imipenem (10 μg), meropenem (10 μg), levofloxacin (5 μg), tetracycline (30 μg), doxycycline (5 μg), cefazolin (30 μg), cefoxitin (30 μg), and ofloxacin (5 μg) (all from Oxoid). In the case of some Gram-positive isolates, vancomycin (30 μg), ampicillin (10 μg), clindamycin (2 μg), and erythromycin (15 μg) were also used. MDR was defined as resistance to at least one antibiotic in at least three antimicrobial categories.[53]

2.4.4. Antimicrobial bioassay. Antibacterial and antifungal assays were performed with Mueller–Hinton agar and Sabouraud dextrose agar medium. Bacterial and fungal cultures were prepared to 0.5 McFarland standards. The antimicrobial activity of Cur-CuO NPs and CS-CuO NPs was evaluated by disc diffusion assay against Gram-negative bacteria, such as *Klebsiella pneumoniae*, *Escherichia coli*, *Pseudomonas aeruginosa*, *Acinetobacter baumannii*, *Proteus mirabilis* and *P. vulgaris*, and Gram-positive bacteria, such as *Enterococcus faecalis*, *Staphylococcus aureus* MSSA, *Staphylococcus aureus* MRSA, and *Streptococcus pyogenes*, and *C. albicans*. 100 μL of the standardized culture of each tested microorganism was spread on the surface of the agar plates using a sterile glass spreader. Filter discs (6 mm) were sterilized and saturated with different concentrations of nanoparticles (10, 25, and 50 μL), dried, and placed on the culture plate. Bacterial and fungal cultures were incubated at 37 °C and 28 °C for 24 h for bacterial and fungal isolates, respectively. In addition, *C. longa* ethanolic (turmeric) extract and chitosan were utilized as control samples to elucidate the proposed antimicrobial efficacy compared to curcumin-capped copper oxide NPs and chitosan-capped copper oxide NPs, respectively. After incubation, the plates were observed for antimicrobial activities by determining the diameters of the formed inhibition zones for each sample. The disc diffusion assay was performed in triplicate.

2.4.5. Minimum inhibitory concentration test. Minimum inhibitory concentration (MIC) is determined as the lowest concentration that completely inhibits bacterial growth after incubation, as measured by the observed turbidity in a test tube.[54] Serial two-fold dilutions of copper nanoparticles were prepared with concentrations of 1000, 500, 250, 125, 62.5, 31.25, 15.62, 7.81, and 3.9 μg mL^{-1}, respectively, with adjusted bacterial and fungal concentrations (10^8 CFU mL^{-1}, 0.5 McFarland's standard) to determine their MIC in BHI broth. 100 μL of 10^8 CFU mL^{-1} of each tested microorganism was pipetted into each test tube and incubated at 37 °C for 24 h. The broth inoculated with bacteria was used as a positive control, whereas BHI broth containing the nanoparticles was used as a negative control.

2.4.6. Detection of ROS in bacterial cell. The intracellular ROS was estimated using the DCFH-DA method.[55] The treated bacterial cell suspensions were centrifuged at 4 °C for 30 min at 300 g, and the supernatant was treated with 100 μM DCFH-DA for 1 h. The intensity was recorded using a 5010 V5+ spectrophotometer (Germany) with wavelength of 485 and 530 nm.

2.5. Biocompatibility assay

2.5.1. Cell culture. In the present study, human lung fibroblasts (WI38) as the testing cell line model were obtained

Table 1 Clinical sources of microbial isolates

Source of microorganism isolates	*S. aureus* MSSA	*S. aureus* MRSA	*P. aeruginosa*	*K. Pneumoniae*	*A. baumannii*	*P. mirabilis*	*P. vulgaris*	*E. coli*	*E. faecalis*	*S. Pyogenes*	*C. albicans*
Sputum	0	3	0	5	1	0	0	2	0	0	0
Urine	4	0	6	11	3	2	1	7	4	0	5
Wound	5	11	9	12	5	3	2	7	3	2	2
Blood	1	5	0	5	1	0	0	1	0	0	0

from ATCC (American Tissue Culture Collection) *via* the Holding Company for Biological Products and Vaccines (VACSERA), Cairo, Egypt. A confluent layer of the used cell line was maintained in Roswell Park Memorial Institute (RPMI) 1640 medium supplemented with 10% fetal bovine serum (Biowest). Antibiotics of 100 units per mL penicillin and 100 μg per mL streptomycin were added at 37 °C in a 5% CO_2 incubator. The cell lines were seeded in a 96-well plate at a density of 1.0×10^4 cells per well at 37 °C for 48 h under 5% CO_2, as reported in the protocol by Schmidt.[56] Then, a hemocytometer was used to count the sub-cultured cells that were plated on the 96-well plate.[4,57]

2.5.2. MTT assay. Based on the protocol reported by El-Kattan *et al.*,[4] both CS- and Cur-capped CuO NPs were sterilization by irradiation under UV light for 3 h before application. Then serial dilutions of 1.56, 3.125, 6.25, 12.5, 25, 50, and 100 μg mL^{-1} of CS-capped CuO NPs and Cur-capped CuO NPs dispersed in 2% RMPI-1640, respectively, were prepared. In addition, doxorubicin (DOX) was employed as a negative control sample. The biocompatibility of the CS-capped CuO NPs and Cur capped CuO NPs was tested *via* the MTT assay against human lung fibroblasts (WI38) *via* colorimetric assay based on the conversion of the yellow tetrazolium bromide (MTT) to a purple formazan derivative by mitochondrial succinate dehydrogenase in viable cells. After incubation, the cells were treated with different concentrations of compounds and incubated for 24 h. After 24 h of drug treatment, 20 μL of MTT solution at 5 mg mL^{-1} was added and incubated for 4 h. Dimethyl sulfoxide (DMSO) in the volume of 100 μL was added to each well to dissolve the purple formazan formed. The colorimetric assay was measured and the absorbance at 570 nm recorded using a plate reader (EXL 800, USA). The relative cell viability in percentage was calculated as follows:

$$\text{Cell viability } \% = \frac{A_{570}(\text{treated sample})}{A_{570}(\text{untreated sample})} \times 100$$

where A_{570} is the optical absorbance obtained at the wavelength of 570 nm for both the treated and untreated cell lines.[58,59]

2.6. Statistical analysis

The statistical analysis was performed using IBM SPSS (version 25) with a population at ($P < 0.05$) and ($P < 0.01$) compared to the control. The experiments were conducted in triplicate and expressed as mean ± SD. Significant differences among means were evaluated using Duncan's multiple range or one-way ANOVA test.

3. Results and discussion

3.1. Identification of the ethanolic extract of turmeric (*Curcuma longa* Linn) powder

The validation of for the ethanolic extract of *Curcuma longa* Linn (*i.e.*, *C. longa*) against pure (standard) curcumin was achieved as illustrated in our previously published work.[4] The UV-vis spectra of *C. longa* ethanolic extract and pure (standard) curcumin showed a single broad band with the maximum absorbance

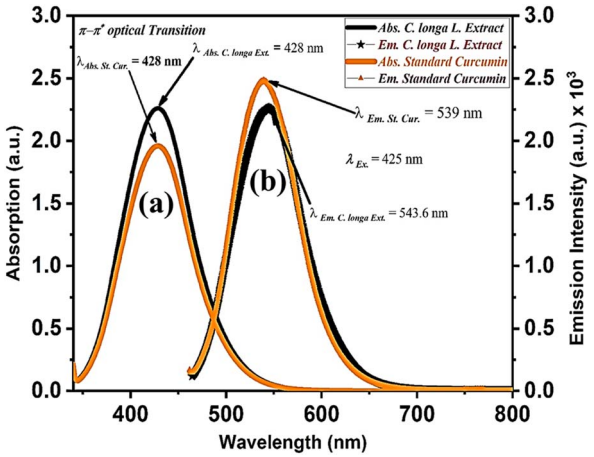

Fig. 1 Validation process using (a) UV-vis absorption and (b) emission spectra of *C. longa* ethanolic extract (black line) against standard pure curcumin (orange line).

peak at 426 nm, which is attributed to low energy π–π* excitation. In addition, pure (standard) curcumin showed a single narrow emission band at 539 nm, as shown in Fig. 1. Alternatively, the *C. longa* ethanolic extract also showed a single narrow emission band, but with a slight shift at 543 nm depending on the sample, which is consistent with previous reports (see Fig. 1).[60–62] The TLC bands of both pure curcumin and the ethanolic extract of *Curcuma longa* Linn (*i.e.*, *C. longa*) powder were observed after 1 h of exposure to mobile phase vapor. The standard pure curcumin showed a single TLC band after irradiation to UV light at a wavelength of 366 nm (see Fig. 2).[63] Alternatively, the ethanolic extract of *C. longa* showed two bands, as shown in Fig. 2. The upper band is ascribed to curcumin, while the middle band is demethoxycurcumin, which agree with the study reported by Kamble and Dahake Pavan.[64]

In addition, a study using gas chromatography-mass spectrometry (GC-MS) was conducted on the ethanolic extract of *Curcuma longa* Linn (turmeric) powder *vs.* pure curcumin to show their chemical composition. This study found ten different chemicals in the pure curcumin purchased from Herbal House Center, Egypt – (Lot No. HHC092021), and their

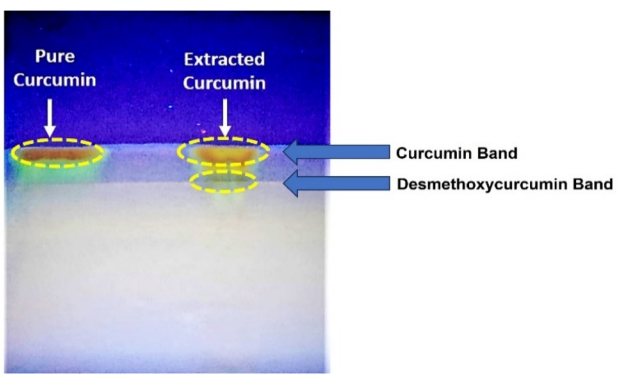

Fig. 2 TLC visual bands of pure standard curcumin (left side) and ethanolic extract of *C. longa* (right side).

Table 2 GC-MS analysis of pure curcumin ethanolic solution

Peak	RT	Name	Formula	Area	Area sum %
1	23.519	2-Methoxy-4-vinylphenol	$C_9H_{10}O_2$	3 289 710.7	1.85
2	38.371	3-Buten-2-one, 4-(4-hydroxy-3-methoxyphenyl)-	$C_{11}H_{12}O_3$	12 954 073.27	7.77
3	42.263	*n*-Hexadecanoic acid	$C_{16}H_{32}O_2$	61 189 184.17	32.4
4	46.358	9-Octadecenoic acid, (*E*)-	$C_{18}H_{34}O_2$	72 579 212.42	37.51
5	46.434	Curlone	$C_{15}H_{22}O$	3 528 061.47	2.12
6	46.85	Oleic acid	$C_{18}H_{34}O_2$	6 825 001.8	4.09
7	54.315	Bis(2-ethylhexyl)phthalate	$C_{24}H_{38}O_4$	6 344 755.35	3.7
8	57.68	Ar-turmerone	$C_{15}H_{20}O$	11 724 070.17	6.23
9	61.96	Borneol, pentafluoropropionate	$C_{13}H_{17}F_5O_2$	3 179 711.5	1.23
10	62.58	(+)-Alpha-curcumene	$C_{15}H_{22}$	6 321 477.21	3.1

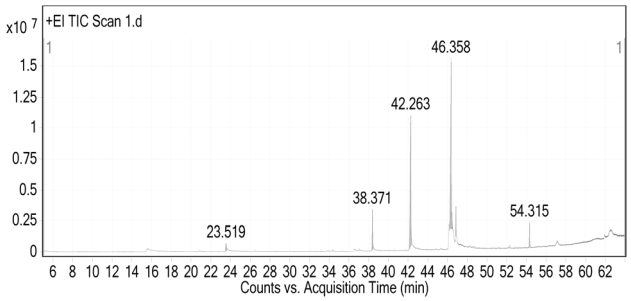

Fig. 3 GC-MS/MS chromatogram of all the identified compounds in pure curcumin extract.

bioactive chemicals, retention time (RT), peak areas (%), and molecular formulas are listed in Table 2. The main chemicals found were 9-octadecenoic acid, (*E*)-(37.51%), *n*-hexadecanoic acid (32.4%), and 3-buten-2-one, 4-(4-hydroxy-3-methoxyphenyl) (7.77%), which are consistent with previous findings, as shown in the chromatogram illustrated in Fig. 3 and S1–S3 in the ESI,† respectively.[65,66]

Alternatively, the gas chromatography-mass spectrometry chromatogram of the ethanolic extract from *Curcuma longa* Linn (turmeric) powder identified 26 compounds, as shown in Table 3, Fig. 4 and S4–S8 in the ESI.† The major molecules were Ar-turmerone (30.39%), followed by curlone (12.33%), 9-octadecenoic acid, (*E*)-(9.77%), *n*-hexadecanoic acid (7.62%), and 3-buten-2-one, 4-(4-hydroxy-3-methoxyphenyl)-(7.38%). Earlier studies also identified the majority of turmerones,[67–71] which are terpenoid chemicals and are important components of the *Curcuma* species.[72] These components have a variety of pharmacological activities, including antibacterial, antioxidant, and anti-inflammatory properties.[72] The bioactive components of

Table 3 GC-MS/MS analysis of the ethanolic extract of *Curcuma longa* Linn (turmeric) powder

Peak	RT	Name	Formula	Area	Area sum %
1	12.991	*p*-Cymene	$C_{10}H_{14}$	699 955.52	0.35%
2	23.511	2-Methoxy-4-vinylphenol	$C_9H_{10}O_2$	1 542 020.92	0.78%
3	24.857	Eugenol	$C_{10}H_{12}O_2$	803 411.42	0.41%
4	26.386	Vanillin	$C_8H_8O_3$	825 515.89	0.42%
5	28.938	(+)-Alpha-curcumene	$C_{15}H_{22}$	2 517 379.14	1.27%
6	30.244	Cyclohexene, 3-(1,5-dimethyl-4-hexenyl)-6-methylene-, [*S*-(*R**, *S**)]-	$C_{15}H_{24}$	629 517.91	0.32%
7	31.892	Benzene, 1,1′-(1,1,2,2-tetramethyl-1,2-ethanediyl)bis-	$C_{20}H_{26}$	2 054 993.87	1.04%
8	34.358	Ar-turmerone	$C_{15}H_{20}O$	60 029 102.04	30.39%
9	35.4	Curlone	$C_{15}H_{22}O$	20 966 625.58	12.33%
10	36.504	1-(4-Hydroxybenzylidene)acetone		3 605 314	2.69%
11	37.09	Dicumyl peroxide	$C_{18}H_{22}O_2$	5 622 002.45	2.85%
12	37.338	6-Isopropenyl-4,8*a*-dimethyl-4*a*,5,6,7,8,8*a*-hexahydro-1*H*-naphthalen-2-one	$C_{15}H_{24}O$	4 483 499.65	2.27%
13	37.833	4,4-Diallyl-cyclohexanone	$C_{16}H_{24}O_6$	1 845 258.02	0.93%
14	37.897	Borneol, pentafluoropropionate	$C_{13}H_{17}F_5O_2$	3 998 162.43	2.02%
15	38.362	3-Buten-2-one, 4-(4-hydroxy-3-methoxyphenyl)-	$C_{11}H_{12}O_3$	14 575 091.99	7.38%
16	40.175	1-Adamantanecarboxylic acid, 3-phenylpropyl ester	$C_{17}H_{20}O_2$	6 724 212.31	3.4%
17	40.595	1-Methoxybicyclo[2,2,2]oct-5-en-2-yl methyl ketone	$C_{11}H_{16}O_2$	3 381 998.35	1.71%
18	41.075	2,2,6-Trimethyl-1-(3-methylbuta-1,3-dienyl)-7-oxabicyclo[4.1.0]heptan-3-ol	$C_{14}H_{22}O_2$	1 040 626.31	0.53%
19	41.518	(*E*)-2-Isopropyl-5-methylphenyl 2-methylbut-2-enoate	$C_{15}H_{22}O_2$	5 069 205.11	2.57%
20	42.176	*n*-Hexadecanoic acid	$C_{16}H_{32}O_2$	15 062 805.96	7.62%
21	42.82	3-Methyl-but-2-enoic acid, 1,7,7-trimethyl-bicyclo[2.2.1]hept-2-yl ester	$C_{15}H_{26}O_2$	3 307 390.87	1.67%
22	46.104	9,12-Octadecadienoic acid (*Z*,*Z*)-	$C_{18}H_{32}O_2$	2 799 112.78	1.42%
23	46.282	9-Octadecenoic acid, (*E*)-	$C_{18}H_{34}O_2$	19 306 924.05	9.77%
24	46.812	Oleic acid	$C_{18}H_{34}O_2$	2 710 804.34	1.37%
25	54.314	Bis(2-ethylhexyl) phthalate	$C_{24}H_{38}O_4$	5 609 218.7	2.84%
26	61.9	1-Heptatriacotanol	$C_{37}H_{76}O$	1 829 870.02	1.65%

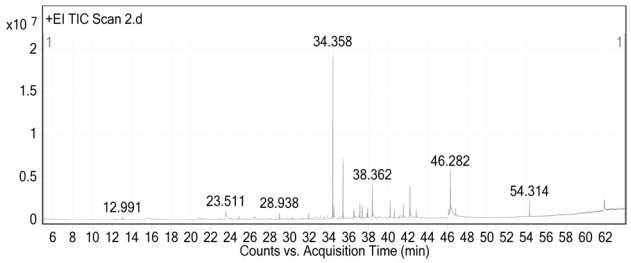

Fig. 4 GC-MS/MS chromatogram of all the identified compounds in the ethanolic extract from *C. longa* (Turmeric) powder.

Curcuma longa are responsible for its medicinal properties, according to the findings of Anekwe *et al.*[73] Furthermore, the chemical makeup of the turmeric rhizome is determined by its genotype, field circumstances, and postharvest processing.[74]

3.2. Characterization of curcumin capped- and chitosan capped-copper nanoparticles

The photophysical properties of the as-prepared Cur-CuO NPs and CS-CuO NPs were investigated by monitoring their UV-vis absorption spectra, as shown in Fig. 5. Cur-CuO NPs exhibit a single broad absorption band at 400 nm and a noticeable shoulder at 460 nm, showing the existence of copper oxide nanoparticles capped with curcumin extract (Cur-CuO NPs) (see Fig. 5, black line). Alternatively, the chitosan-capped copper oxide nanoparticles (CS-CuO NPs) showed a characteristic feature at the shoulder at 370 nm, indicating the formation of CS-CuO NPs (see Fig. 5, red line), which agrees with previous studies.[40,46] Moreover, the morphological properties, including the particle size and shape of Cur-CuO and CS-CuO NPs, are depicted in Fig. 6. Both the green-synthesized Cur-CuO and CS-CuO NPs show quasi-spherical-like particles with average sizes of 25 ± 10 nm (Fig. 6a and b) and 10 ± 5 nm (Fig. 6c and d), respectively.

The EDX spectra show Cu and O as the main elemental composition, indicating the purity of the CS-CuO and Cur-CuO

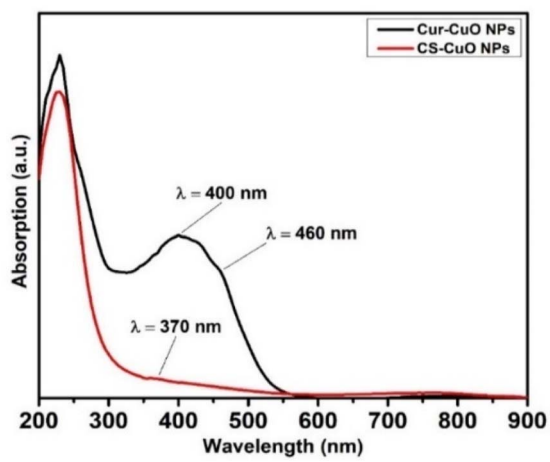

Fig. 5 Absorption spectra of Cur-CuO NPs (black line) and CS-CuO NPs (red line).

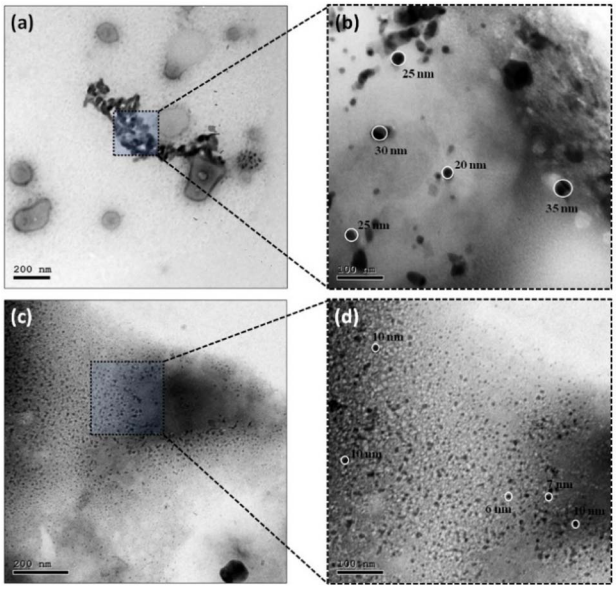

Fig. 6 TEM images of Cur-CuO NPs (a and b) and CS-CuO NPs (c and d).

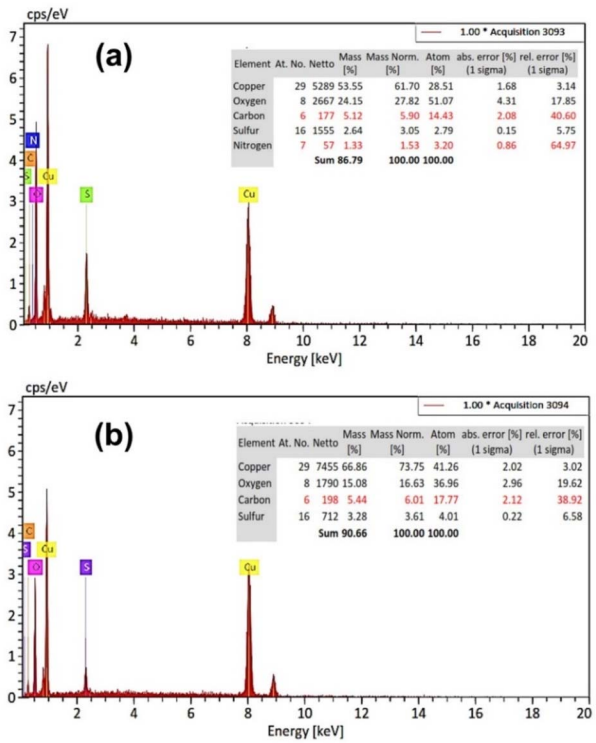

Fig. 7 EDX analysis of CS-CuO NPs (a) and Cur-CuO NPs (b).

NPs samples, as shown in Fig. 7. The atomic percentage of copper (Cu) and oxygen (O) in CS-CuO NPs was about 28.51% and 51.07%, respectively. The atomic percentage of copper (Cu) and oxygen (O) in Cur-CuO NPs was about 41.26% and 36.96%, respectively. In addition, the presence of nitrogen and carbon in the EDX spectrum of CS-CuO NPs is attributed to the amino groups and carbon present in chitosan (see Fig. 7a). Besides, the

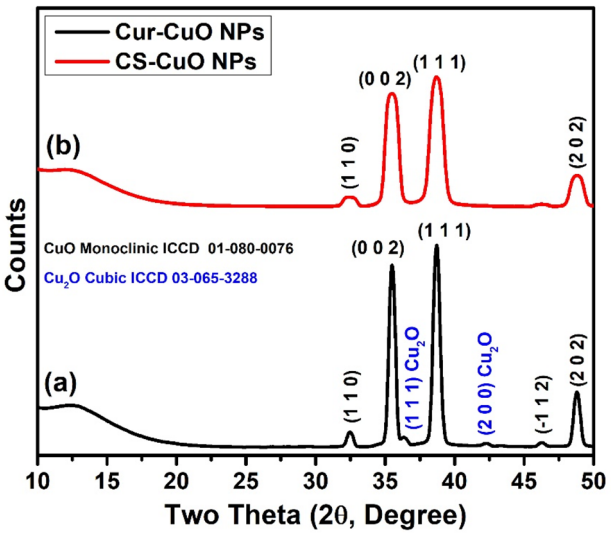

Fig. 8 XRD patterns of (a) Cur-CuO NPs (black line) and (b) CS-CuO NPs (red line).

EDX spectrum of Cur-CuO NPs displayed the presence of copper, oxygen and carbon elements, indicating the formation of Cur-CuO NPs (see Fig. 7b). Moreover, the EDX spectra of CS-CuO and Cur-CuO NPs clearly explained the fact that the amount of Cu decreased with a decrease in the CuO content in these hybrid nanocomposites. Finally, the presence of sulfur (S) element is due to the inorganic nature of the copper precursor (*i.e.*, copper sulfate, $CuSO_4$).

Fig. 8 presents the X-ray diffraction (XRD) patterns of the curcumin-capped CuO nanoparticles (Cur-CuO NPs) (see Fig. 8a) and chitosan-capped CuO nanoparticles (CS-CuO NPs), as shown in Fig. 8b.

The XRD pattern of Cur-CuO NPs shows the presence of both monoclinic CuO (ICCD 01-080-0076) and cubic Cu_2O (ICCD 03-065-3288) calculated as diffraction peaks with a change in 2θ (see Fig. 8a). The strongest peaks are found at the 2θ values of 35.5° and 38.7°, which correspond to the (1 1 0) and (1 1 1) planes, respectively. The other peaks corresponding to the (1 1 0), (2 0 2), and (0 2 0) planes are located at around 32.5°, 48.7°, and 53.5°, respectively. In addition, another two diffraction patterns, specifically the (1 1 1) and (2 0 0) planes that characterize to Cu_2O crystal phases, are distinctly visible in the XRD pattern of the CuO/Cu_2O NPs sample. The average crystallite size was calculated to be 14.35 nm. The XRD pattern for CS-CuO NPs (see Fig. 8b) exhibits almost the same major peaks at around 35.5° and 38.7° for the (0 0 2) and (1 1 1) planes of a monoclinic CuO. A peak is observed also for the (2 0 2) plane at around 48.7°. CS-CuO NPs exhibits a stronger and broader diffraction pattern than curcumin-capped Cu_2O, supporting the conclusion that they have a smaller particle size. The average crystallite size was about 4.59 nm, which is smaller than that of CS-CuO NPs, and in good agreement with the TEM data.

The large background observed in both patterns, especially in the low 2θ range (10–20°), is attributed to presence of amorphous constituents such amorphous capping ligands (curcumin and chitosan).

In addition, colloidal properties, including dynamic light scattering (DLS) and electrophoretic mobility based on zeta

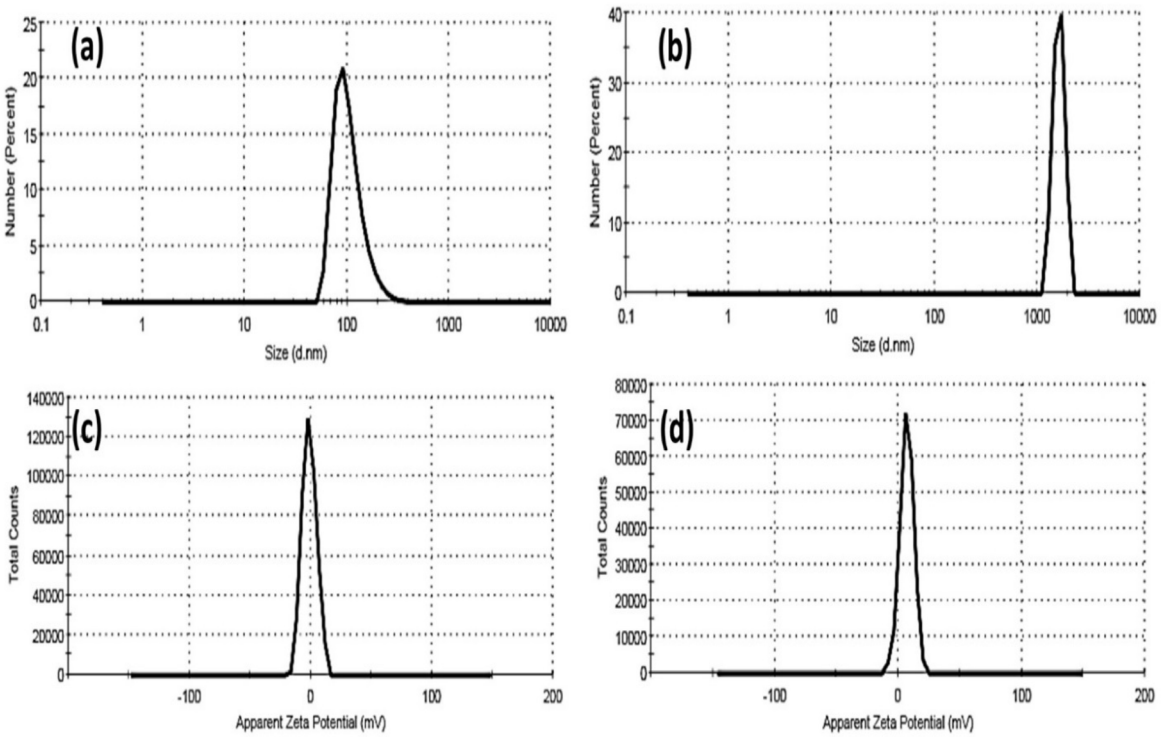

Fig. 9 DLS data of Cur-CuO NPs (a) and CS-CuO NPs (b). Zeta potential of Cur-CuO NPs (c) and CS-CuO NPs (d).

Table 4 Colloidal properties of Cur-CuO NPs and CS-CuO NPs at 0 time and after storage for 12 months

	Dynamic light scattering (DLS)		
Sample	Hydrodynamic diameter (H_D, nm)	Polydispersity index (PDI)	Zeta potential (ζ, mV)
Cur-CuO NPs (0 Time)	105.1 ± 36.58	0.28	−1.07
Cur-CuO NPs (12 Months)	107.7 ± 19.26	0.79	−4.39
CS-CuO NPs (0 Time)	1631 ± 205.5	0.698	+7.1
CS-CuO NPs (12 Months)	1319 ± 208	0.599	+2.44

potential measurements, were investigated for Cur-CuO NPs and CS-CuO NPs in a vehicle solution, as shown in Fig. 9 and Table 4. The hydrodynamic diameter (H_D) of Cur-CuO NPs was about 105.1 ± 36.58 nm with a polydispersity index (PDI) of 0.28, which is smaller than that of CS-CuO NPs. The average H_D of CS-CuO NPs was about 1631 ± 205.5 nm with a more extensive polydispersity index (PDI) of 0.698 (Fig. 9a and b and Table 4). The zeta potential of Cur-CuO NPs was about −1.07 mV, which is lower than the zeta-potential of the CS-CuO NPs, with a value of about +7.1 mV, as shown in Fig. 9c and d, respectively, and Table 4. According to the previously mentioned colloidal properties based on the DLS data, the hydrodynamic particle size of the as-prepared nanoparticles is enlarged, consistent with their agglomeration. This agglomeration is because of their hydrophilicity. In addition, the intensity of the steric forces of the functional groups on the surface of the nanoparticles is generated by creating a layer of water around the material.

Furthermore, the surface properties of Cur-CuO NPs and CS-CuO NPs were investigated *via* Fourier-transform infrared (FT-IR) based on their transmittance as a function of wavenumber, as shown in Fig. 10. The FT-IR spectrum of Cur-CuO NPs showed a strong stretching band at a wavenumber of 3401 cm^{-1} due to the presence of –OH intermolecular bonded alcohol in the ethanolic solution or the phenolic components in the turmeric extract. Two stretching aliphatic –CH bands were observed at 2977 and 2896 cm^{-1}, corresponding to the sp^2 C–H bond existing in $–OCH_3$ (*i.e.*, methoxy) groups in the curcumin component.[75–77] Also, the asymmetric stretching vibration at 2348 cm^{-1} indicates the presence of the O=C=O group due to the decarboxylation of the phenolic compounds ferulic acid and its derivatives such as 3-buten-2-one, 4-(4-hydroxy-3-methoxyphenyl) (*i.e.*, feruloylmethane) present in the turmeric extract and the –COOH attached to their aromatic ring (see Fig. 10, black line).[78,79] In addition, the stretching strong vibration at 1635 cm^{-1} is assigned to C=O in the β-diketone moiety (O=C–CH=CH–C=O) and C–H bending frequency of the aromatic overtone, which are present in turmeric extract flavonoids such as curcumin, and other curcuminoid compounds present in turmeric, such as demethoxycurcumin and bisdemethoxycurcumin.[76,77] The symmetric bending band at 1379 cm^{-1} is due to the vibration of the $–CH_3$ group present in the flavonoids in the turmeric ethanolic extract.[80] The weak stretching band of aromatic C–O enol and bending phenolic –OH group of the curcuminoid components are assigned to the peak at 1272 cm^{-1}. The sharp stretching band at 1052 cm^{-1} is assigned to the C–O–C stretching vibration of phenyl alkyl ether, which confirmed the molecular structure of curcumin and other curcuminoid components extracted from turmeric.[81] The weak stretching band at 663 cm^{-1} corresponds to Cu–O as a result of the interaction between the turmeric extract components and copper oxide surface.[81,82] Finally, the weak sharp band at 879 cm^{-1} is attributed to the aromatic C–H out-of-plane bending vibration in curcumin and other curcuminoid components.[77]

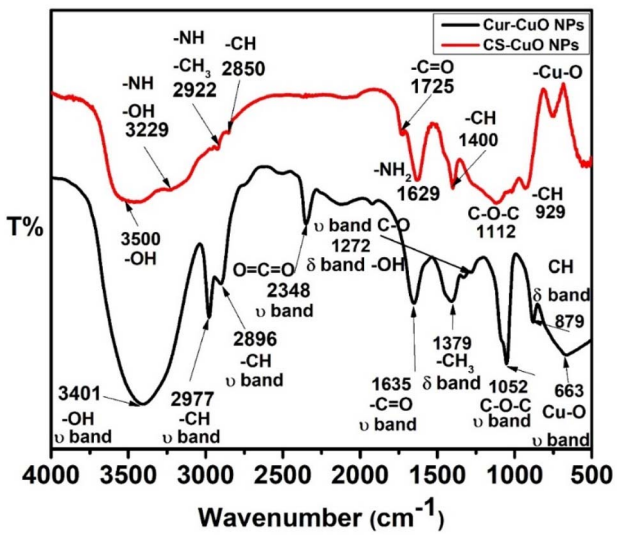

Fig. 10 FT-IR spectra of Cur-CuO NPs (black line) and CS-CuO NPs (red line).

Alternatively, CS-CuO NPs, as shown in Fig. 10 (red line), showed the characteristic peaks for chitosan at 3500 and 1112 cm^{-1}, corresponding to the –OH and –C–O–C– stretching vibrations, respectively. The $–NH_2$ bending vibration peak was observed in chitosan at 1629 cm^{-1}. The peaks at 2922 cm^{-1} correspond to the stretching vibration of $–CH_3$ and –NH, and the peak at 1400 cm^{-1} belongs to the stretching vibration of the C–H bond. In addition, the stretching band of C–O in the spectrum of chitosan was observed at 894 cm^{-1} due to the conjugation with Cu–O. According to the comparison between the FTIR spectra of Cur-CuO and CS-CuO NPs, two characteristic features are observed at 2977 and 2896 cm^{-1} in Cur-CuO NPs than CS-CuO NPs due to the stretching vibration of –CH of alkyne in the curcumin molecule and intermolecular-bonded –OH alcohol that exists in the ethanolic solution, respectively. The second difference was observed at 2348, 1920, and

1052 cm^{-1} due to the medium stretching bands for the –O═C═O–, –CCC– and –C–O groups existing in curcumin and primary alcohol, respectively. The last difference observed at 3229, 2850 and 1725 cm^{-1} in CS-CuO compared to Cur-CuO NPs due to –NH_2 of chitosan, –CH, C═O of aliphatic ketone, and –OH group in carboxylic acid.[40] Furthermore, the sharp band at 1634 cm^{-1} and less intense band at 1377 cm^{-1} are attributed to the M–O out-of-plane rocking and in-plane rocking, respectively.[40]

3.3. Evaluation of the long-term stability and shelf-life of Cur-CuO and CS-CuO NPs

Stability is essential for determining the usefulness of nanoparticles in real-life applications such as biomedicine, catalysis, and environmental science. Thus, a 12-month stability study was conducted considering parameters such as hydrodynamic diameter (H_D), polydispersity index (PDI), and zeta potential using DLS, as shown in Table 4. The findings reveal that Cur-CuO NPs only exhibited small variations in size, which slightly changed from 105.1 ± 36.58 nm to just 107.7 ± 19.26 nm. However, their PDI increased from 0.28 to 0.79, indicating that this system was becoming increasingly heterogeneous, which demonstrates the growth of some relatively small aggregates. Moreover, the zeta potential became more negative (−1.07 mV to −4.39 mV), suggesting that changes in surface charge interactions and colloidal stability occurred. However, despite the slight changes in size, the resulting data confirmed the sufficient size stability of the Cur-CuO NPs and proved their decent shelf-life (see Table 4).

Alternatively, the CS-CuO NPs exhibited a rather substantial reduction in hydrodynamic diameter from 1631 ± 205.5 nm to 1319 ± 208 nm, which is probably due to the structural changes or partial sedimentation of the large nanoparticle aggregates over time. The PDI showed a decrease in value from 0.698 to 0.599, denoting that the size uniformity improved slightly. Nevertheless, the zeta potential decreased from the previous level of +7.1 mV to +2.44 mV, indicating that there was less repulsion between the particles, which might be one reason for their instability. On the negative side, the zeta potential was between −10 mV and +10 mV, which shows that CS-CuO NPs are more likely to form aggregates after some time. These results are consistent with former investigations showing that particles with a larger initial size and smaller surface charge present higher risks of sedimentation and aggregation, as shown in Table 4.[83]

The capping agents are responsible for the dissimilarity in the long-term stability of the Cur-CuO and CS-CuO NPs. Curcumin, a nanoparticle-stabilizing agent, is superior due to its stabilizing action, which allows the nanoparticles to stay dispersed and resistant to head-to-head aggregation.[84] Alternatively, chitosan deposits at the beginning of the reaction, given that it is positively charged, showing stability for a short time. Nonetheless, it may be highly likely that its dispersion may be hampered or even lost because of its destruction due to structural degradation or deterioration of electrostatic interactions. Alternatively, PDI values below the threshold of 0.3 can be overtly stable nanoparticles, and numbers above 0.7 can mean aggregation. The increase in the PDI of Cur-CuO and the CS-CuO zeta decrease in potential are the main signs causing us to believe that they undergo degradation processes, but with Cur-CuO showing better long-term stability.[85]

3.4. Distribution and prevalence of clinically isolated pathogenic bacteria

One hundred eighty specimens were collected from different sources from patients diagnosed with diverse infections, as shown in Table 5. Among the sources sampled, 128 (71.1%) had pathogenic microbial growth. After the isolation and characterization, the results showed that the most frequent isolated pathogenic bacteria were *Klebsiella pneumoniae* accounting for 33 strains (25.8% of total isolated strains), followed by *Staphylococcus aureus* (MRSA), which gave a frequency of 19 strains (14.8%). Ten strains (7.8%) were *Staphylococcus aureus* (MSSA).

Moreover, *Escherichia coli* and *Pseudomonas aeruginosa* were present with a frequency of 17 strains (13.3%) and 15 (11.7%), respectively. *Acinetobacter baumannii* was present, recording 10 strains (7.8%), whereas *Enterococcus faecalis* had 7 strains (5.5%). In the case of the *Proteus* genus, 5 strains (3.9%) were *Proteus mirabilis*, and 3 strains (2.3%) were *Proteus vulgaris*. Finally, the lowest recorded bacteria were *Streptococcus pyogenes*, accounting for 2 strains (1.6%). However, *Candida*

Table 5 Frequency of pathogenic microorganisms isolated from clinical specimens

Category	Organisms	No. of strains	Frequency %
Gram-positive bacteria	*Enterococcus faecalis*	7	5.5
	Staphylococcus aureus MSSA	10	7.8
	Staphylococcus aureus MRSA	19	14.8
	Streptococcus pyogenes	2	1.6
Gram-negative bacteria	*Klebsiella pneumoniae*	33	25.8
	Escherichia coli	17	13.3
	Pseudomonas aeruginosa	15	11.7
	Acinetobacter baumannii	10	7.8
	Proteus mirabilis	5	3.9
	Proteus vulgaris	3	2.3
Fungi	*Candida albicans*	7	5.5
Total		128	100

albicans accounts for 7 strains (5.5%). Our findings agree with previous reports,[84,86] stating that the most frequently distributed bacteria were Gram-negative bacteria compared with Gram-positive bacteria and the presence of *Candida albicans* in intensive care units.

3.5. Antibiotic inhibition capacity

The antibiotic resistance capacities of the isolated microorganisms were investigated against 21 antibiotic discs, as shown in Table 6. The results revealed that methicillin-sensitive *S. aureus* (MSSA) strains resisted cefotaxime and ofloxacin. Nevertheless, they showed strong resistance against ampicillin, ceftazidime, levofloxacin, doxycycline, and erythromycin with values of 90%, 80%, 80%, 80% and 70%, respectively. MSSA also showed moderate resistance, with 60% against amikacin and gentamicin and 50% against ampicillin/sulbactam, ciprofloxacin, tetracycline, and clindamycin. Moreover, MSSA showed moderate to weak resistance against amoxycillin/clavulanic acid, cefazolin, cefepime, and tigecycline with values of 40%, 40%, 30% and 20%, respectively. Conversely, MSSA was completely sensitive to vancomycin. The methicillin-resistant *S. aureus* (MRSA) strains showed 100% resistance against 14 out of the 21 tested antibiotics, which are amoxycillin/clavulanic acid, ampicillin/sulbactam, cefazolin, cefepime, cefotaxime, ceftazidime, cefoxitin, gentamicin, imipenem, meropenem, levofloxacin, ofloxacin, ampicillin, and erythromycin. However, MRSA showed strong to moderate resistance against clindamycin, tetracycline, doxycycline, amikacin, ciprofloxacin, and tigecycline, recording 84.2%, 68.4%, 63.2%, 52.6% and 36.8% resistance, respectively. Only vancomycin was shown to be effective against 100% of the MRSA strains.

Our results are consistent with previous reports[87,88] stating that *S. aureus* is one of the most prevalent pathogenic bacteria that frequently resist multiple drugs, contributing to various infections. Methicillin-resistant *S. aureus* (MRSA) is particularly concerning, which substantially impacts antimicrobial resistance levels across numerous countries. The *S. aureus*-acquired resistance against various antibiotics is attributed to genetic factors and mutations.[89,90] *E. faecalis* showed complete resistance (100%) against cefotaxime, cefoxitin, and ampicillin, as previously reported.[4,91] Nevertheless, *E. faecalis* exhibited strong resistance, accounting for 85.7% against ampicillin/sulbactam, ceftazidime, ofloxacin, and doxycycline; 71.4% against amikacin, cefazolin, gentamicin, and clindamycin; and 57.1% against amoxycillin/clavulanic acid, cefepime, ciprofloxacin, levofloxacin, and erythromycin. Moreover, as previously stated, weak resistance was observed against tigecycline and vancomycin, recording 14.3% resistance.[92] Imipenem and meropenem antibiotics efficiently killed 100% of *E. faecalis*. The obtained results are consistent with previous reports stating that *E. faecalis* is considered one of the most dangerous multidrug resistant bacteria, and the acquired resistance is attributed to its high capacity in transferring and acquiring antibiotic resistance genes through mobile genetic elements such as plasmids.[53,93]

S. pyogenes demonstrated 100% resistance against 11 antibiotics (amikacin, amoxycillin/clavulanic acid, ampicillin/sulbactam, cefazolin, cefotaxime, cefoxitin, ciprofloxacin, doxycycline, ofloxacin, ampicillin, and erythromycin). The results agree with that obtained by Yu and co-workers,[94] stating

Table 6 Antibiotic resistance pattern (%) of bacterial isolates

Antibiotic discs	*S. aureus* MSSA	*S. aureus* MRSA	*E. faecalis*	*S. pyogenes*	*A. baumannii*	*E. coli*	*K. pneumoniae*	*P. vulgaris*	*P. mirabilis*	*P. aeruginosa*
Amikacin (30 μg)	60	63.2	71.4	100	70	29.4	72.7	33.3	60	66.7
Amoxycillin/clavulanic acid (30 μg)	40	100	57.1	100	80	88.2	100	100	100	100
Ampicillin/sulbactam (30 μg)	50	100	85.7	100	80	64.7	100	100	80	80
Cefazolin (30 μg)	40	100	71.4	100	100	82.4	100	66.7	60	86.7
Cefepime (30 μg)	30	100	57.1	50	80	52.9	90.9	33.3	40	100
Cefotaxime (10 μg)	100	100	100	100	90	82.4	100	100	100	100
Ceftazidime (30 μg)	80	100	85.7	50	90	70.6	100	100	100	80
Cefoxitin (30 μg)	0	100	100	100	100	41.2	93.9	100	100	100
Ciprofloxacin (5 μg)	50	52.6	57.1	100	80	82.4	84.8	66.7	80	100
Doxycycline (5 μg)	80	63.2	85.7	100	70	64.7	60.6	100	100	93.3
Gentamicin (10 μg)	60	100	71.4	50	90	41.2	75.8	33.3	40	66.7
Imipenem (10 μg)	0	100	0	50	60	17.6	54.5	0	20	60
Meropenem (10 μg)	0	100	0	0	30	11.8	63.6	0	0	40
Levofloxacin (5 μg)	80	100	57.1	50	50	82.4	75.8	100	80	60
Ofloxacin (5 μg)	100	100	85.7	100	90	52.9	90.9	100	100	80
Tetracycline (30 μg)	50	68.4	28.9	50	50	88.2	66.7	66.7	60	80
Tigecycline (15 μg)	20	36.8	14.3	0	0	0	15.2	0	0	33.3
Ampicillin (10 μg)	90	100	100	100						
Erythromycin (15 μg)	70	100	57.1	100						
Clindamycin (2 μg)	50	84.2	71.4	50						
Vancomycin (30 μg)	0	0	14.3	0						

the strong resistance of *S. pyogenes* against β-lactam antibiotics.[94] In contrast, the other antibiotics showed moderate efficiency, accounting for 50% against *S. pyogenes*, where only tigecycline and vancomycin effectively killed *S. pyogenes*. 100% of *A. baumannii* strains exhibited complete resistance against cefazolin and cefoxitin. However, *A. baumannii* displayed strong resistance ranging from 70% to 90% against several antibiotics, including amikacin, doxycycline, amoxycillin/clavulanic acid, cefepime, cefotaxime, gentamicin, and ofloxacin, where the same observations were reported in a previous study.[95]

Moreover, it exhibited moderate resistance, accounting for 50% against both levofloxacin and tetracycline and 60% against imipenem. *A. baumannii* showed 100% sensitivity against tigecycline.[96] Alternatively, *E. coli* also showed 100% sensitivity against tigecycline, which elucidated the usability of this antibiotic in combating *E. coli*.[97] *E. coli* strains showed different antibiotic resistance capacities ranging between moderate as observed against amikacin, cefoxitin, gentamicin, cefepime, ofloxacin, ampicillin/sulbactam, and doxycycline accounting (29.4%, 41.2%, 41.2%, 52.9%, 52.9%, 64.7% and 64.7%, respectively) to strong resistance, as observed against ceftazidime, cefazolin, ciprofloxacin, cefotaxime, levofloxacin, amoxycillin/clavulanic acid, and tetracycline accounting for 70.6%, 82.4%, 82.4%, 82.4%, 82.4%, 88.2% and 88.2%, respectively. At the same time, it showed weak resistance, 11.8% and 17.6%, against meropenem and imipenem antibiotics, respectively, which agrees with previous reports.[98]

Furthermore, *P. vulgaris* exhibited complete resistance against amoxycillin/clavulanic acid, ampicillin/sulbactam, cefotaxime, ceftazidime, cefoxitin, doxycycline, levofloxacin, and ofloxacin, while moderate resistance of 33.3% was observed with amikacin, cefepime, and gentamicin, and 66.6% with cefazolin, ciprofloxacin, and tetracycline. Imipenem, meropenem, and tigecycline were shown to be effective in combating *P. vulgaris*, resulting in killing 100% of bacteria. Moving forward to the other strain for the Proteus genus *P. mirabilis*, nearly the same resistance patterns were observed, with a slight difference in amikacin accounting for 33.3% resistance compared with 60% observed with *P. vulgaris*. *K. pneumoniae* strains exhibited 100% resistance against 5 tested antibiotics, including amoxycillin/clavulanic acid, ampicillin/sulbactam, cefazolin, cefotaxime, and ceftazidime. Moreover, it showed strong resistance ranging from 60.6% to 93.9% against the other tested antibiotics, and the most interesting observed result was that none of the tested antibiotics showed 100% efficacy against *K. pneumoniae*; however, only tigecycline showed the highest killing capacity against *K. pneumonia* (killing around 84.8% of treated strains), which was the same as previously reported.[99] The obtained results reflected the threats correlated with *K. pneumoniae* as a multi-drug resistant bacteria, agreeing with previous reports.[100,101] Lastly, *P. aeruginosa* was shown to have complete resistance against five antibiotics including amoxycillin/clavulanic acid, cefepime, cefotaxime, cefoxitin, and ciprofloxacin. None of the tested antibiotics were effective against *P. aeruginosa*; however, the lowest recorded resistance obtained was 33.3% against tigecycline.

3.6. Antimicrobial activity of curcumin copper oxide nanoparticles (Cur-CuO NPs)

The antimicrobial activity of the curcumin-capped copper oxide nanoparticles (Cur-CuO NPs) was investigated against clinically isolated pathogens using the disc diffusion assay at three concentrations (*i.e.*, 10 μL–5 μg mL^{-1}; 25 μL–15 μg mL^{-1}; 50 μL–25 μg mL^{-1}, respectively), and the obtained results are presented in Table 7 and Fig. S9–S11 in the ESI.† The results revealed that the three tested concentrations resulted in zones of inhibition against all the investigated pathogenic bacteria together with pathogenic fungi. However, it was noticed that by increasing the concentration of nanoparticles, the observed zone of inhibition was increased, as shown in previously reported studies.[4,45,102] The highest observed zone of inhibition was recorded in the treatment using 50 μL (25 μg mL^{-1}) of Cur-CuO against *Proteus vulgaris*, accounting for 17.3 mm, followed by treatment using the same concentration against one of the most multi-drug resistant (MDR) pathogenic bacteria, *Staphylococcus aureus* (MRSA), which resulted in the appearance of a 16.6 mm inhibition zone, as previously reported.[103] A slightly lower inhibition zone was obtained using 25 μL (15 μg mL^{-1}) against MRSA, recording 14.2 mm. The lowest recorded zone of inhibition was observed against *Staphylococcus aureus* (MSSA) using 10 μL (5 μg mL^{-1}) and 25 μL (15 μg mL^{-1}) of 8.6 and 11 mm, respectively.

The antimicrobial activity of Cur-CuO NPs was investigated by Jayarambabu *et al.*[104] In their study, Cur-CuO NPs were used as suspensions with a concentration of 100, 150, 200 and 250 μL against two bacterial isolates of *Basilus subtilis* (*i.e.*, Gram-positive bacteria) and *Escherichia coli* (Gram-negative bacteria). In their study, the used concentrations were higher than the concentrations used in the current study (*i.e.*, 10 μL–5 μg mL^{-1}; *B*: 25 μL–15 μg mL^{-1}; *C*: 50 μL–25 μg mL^{-1} of Cur-CuO NPs). In addition, the antimicrobial activity was tested against a broad range of bacterial isolates, either Gram-positive or Gram-negative bacteria.

Table 7 Antimicrobial activity of Cur-CuO NPs against pathogenic isolates[a]

	Mean of zone inhibition in mm (mean ± SD)		
Microorganism	*A*	*B*	*C*
Staphylococcus aureus (MSSA)	8.6 ± 0.52	11.0 ± 0.67	14.5 ± 0.53
Staphylococcus aureus (MRSA)	10.6 ± 0.58	14.2 ± 0.69	16.6 ± 0.68
Enterococcus faecalis	10.2 ± 1.07	12.8 ± 0.69	15.1 ± 0.69
Streptococcus pyogenes	10.0 ± 0.0	14.5 ± 0.7	16.5 ± 0.7
Acinetobacter baumannii	10.5 ± 0.7	13.5 ± 0.85	15.4 ± 0.7
Escherichia coli	9.0 ± 0.75	11.3 ± 0.47	14.3 ± 0.59
Klebsiella pneumonia	9.5 ± 0.8	12.2 ± 0.82	15.0 ± 0.91
Proteus mirabilis	10.4 ± 0.55	13.4 ± 0.55	16.0 ± 0.7
Proteus vulgaris	11.0 ± 0.0	14.0 ± 0.0	17.3 ± 0.58
Pseudomonas aeruginosa	10.4 ± 0.91	12.3 ± 0.9	16.4 ± 0.82
Candia albicans	10.4 ± 0.53	14.0 ± 1.0	16.4 ± 0.53

[a] *A*: 10 μL–5 μg mL; *B*: 25 μL–15 μg mL; *C*: 50 μL–25 μg mL^{-1} of Cur-CuO NPs. The diameter of the inhibition zone expressed as mean ± SD (experiment conducted in triplicate), $P < 0.05$ or $P < 0.01$.

Moreover, Cur-CuO NP discs showed efficiency in combating not only pathogenic bacteria but also pathogenic fungi such as *Candida albicans*, where the inhibition zones were monitored using three tested concentrations of Cur-CuO NPs (10.4, 14.0 and 16.4 mm for 10 μL–5 μg mL^{-1}; 25 μL–15 μg mL^{-1}; and 50 μL–25 μg mL^{-1}, respectively), in agreement with previous studies.[105,106] The obtained results give insights into the usability of Cur-CuO NPs against pathogenic bacteria and fungi.[107–109]

3.7. Antimicrobial activity of chitosan copper oxide nanoparticles (CS-CuO NPs)

The antimicrobial activity of the chitosan-capped copper oxide nanoparticles (CS-CuO NPs) was investigated against clinically isolated pathogens, and data are presented in Table 8 and Fig. S12 and S13 in the ESI.† The results showed a variation in the inhibition zones monitored according to the different concentrations of nanoparticles (*i.e.*, 10 μL–5 μg mL^{-1}; 25 μL–15 μg mL^{-1}; 50 μL–25 μg mL^{-1}) and the tested microorganisms. Generally, the antimicrobial effect was strengthened as the concentration of CS-CuO NPs increased in the same manner observed when investigating the Cur-CuO NPs. The highest monitored zone of inhibition of 24.4 mm was observed using 50 μL (25 μg mL^{-1}) of CS-CuO NPs and against *Enterococcus faecalis*. In contrast, the lowest observed zone of inhibition of 10.5 mm was observed for the concentration of NPs of 10 μL (5 μg mL^{-1}) against *Escherichia coli*. Furthermore, CS-CuO NPs were effective in combating the pathogenic fungi *Candida albicans*, resulting in the formation of inhibition zones (12.3, 16.0 and 20.1 mm) for the three concentrations (*i.e.*, 10 μL–5 μg mL^{-1}; 25 μL–15 μg mL^{-1}; 50 μL–25 μg mL^{-1}), respectively. Overall, the inhibition zones were slightly higher than that obtained by Cur-CuO NPs. Our results are consistent with that reported in previous studies.[37,110–112] Furthermore, in the case of chitosan-capped copper oxide nanoparticles (CS-CuO NPs), only two studies have been devoted to investigating their antimicrobial efficacy against bacterial isolates.[37,113] Sathiyavimal *et al.* investigated the antibacterial activity against Gram-positive (*S. pneumoniae* and *S. epidermidis*) and Gram-negative (*E. coli* and *P. mirabilis*) with different concentrations (20, 40, 60, and 80 μg mL^{-1}), which were higher than the concentrations used in the current study (*i.e.*, 5 μg mL^{-1}, 15 μg mL^{-1} and 25 μg mL^{-1} of CS-CuO NPs).[37]

3.8. Plain curcumin and chitosan antimicrobial activity

Antimicrobial activity was investigated to determine whether the antimicrobial effects observed in Table 7 and 8 for Cur-CuO NPs and CS-CuO NPs, respectively, were solely attributed to the copper oxide nanoparticles or the capping materials (curcumin and chitosan), as shown in Table 9 and Fig. S14 and S15 in the ESI,† respectively. The results revealed that plain curcumin did not show any antimicrobial activity against the investigated pathogens, which aligns with the previous report.[4] These results proved that the obtained antimicrobial capacity of Cur-CuO NPs presented in Table 7 was driven by the CuO NPs. However, curcumin can act as a helper in facilitating the diffusion of CuO NPs through the microbe cell membrane due to its hydrophobicity, as previously reported.[114,115] Thus, using plain chitosan resulted in the appearance of inhibition zones for all the investigated pathogenic bacteria and fungi.

In contrast, the highest inhibition zone of 15.2 mm was observed against *Klebsiella pneumonia*, whereas the lowest inhibition zone of 10.3 mm was observed against *Proteus vulgaris*. The antimicrobial capacity of chitosan could result from its polycationic structure, thus electrostatically interacting with the anionic components of the microorganisms,[116] in addition to its hydrophobic and chelating capacities.[117]

The antimicrobial mechanisms of the curcumin-capped copper oxide (Cur-CuO) nanoparticles and chitosan-capped copper oxide (CS-CuO) nanoparticles operate through distinct and complementary pathways, as follows.

Table 8 Antimicrobial activity of CS-CuO NPs against pathogenic isolates[a]

	Mean of zone inhibition in mm (mean ± SD)		
Microorganism	*A*	*B*	*C*
Staphylococcus aureus (MSSA)	14.3 ± 0.48	17.1 ± 0.57	20.5 ± 1.08
Staphylococcus aureus (MRSA)	12.8 ± 1.17	16.4 ± 0.6	19.1 ± 0.94
Enterococcus faecalis	16.1 ± 0.9	20.3 ± 0.76	24.4 ± 0.53
Streptococcus pyogenes	14.0 ± 0.0	16.5 ± 0.7	19.0 ± 0.0
Acinetobacter baumannii	11.0 ± 0.82	14.2 ± 0.42	16.3 ± 0.48
Escherichia coli	10.5 ± 0.62	13.5 ± 0.87	16.2 ± 0.56
Klebsiella pneumonia	11.2 ± 0.85	15.2 ± 0.73	19.5 ± 0.87
Proteus mirabilis	11.6 ± 0.55	15.2 ± 0.45	18.4 ± 0.55
Proteus vulgaris	12.3 ± 0.7	15.0 ± 0.0	19.3 ± 0.58
Pseudomonas aeruginosa	14.4 ± 0.74	17.2 ± 0.94	21.4 ± 1.06
Candia albicans	12.3 ± 0.76	16.0 ± 0.82	20.1 ± 0.69

[a] *A*: 10 μL–5 μg mL; *B*: 25 μL–15 μg mL; *C*: 50 μL–25 μg mL^{-1} of CS-CuO NPs. The diameter of the inhibition zone is expressed as mean ± SD (experiment conducted in triplicate), $P < 0.05$ or $P < 0.01$.

Table 9 Antimicrobial activity of plain curcumin and chitosan against pathogenic isolates[a]

	Mean of zone inhibition in mm (mean ± SD)	
Microorganism	*A*	*B*
Staphylococcus aureus (MSSA)	0.0 ± 0.0	14.2 ± 0.63
Staphylococcus aureus (MRSA)	0.0 ± 0.0	15.0 ± 0.52
Enterococcus faecalis	0.0 ± 0.0	15.1 ± 0.38
Streptococcus pyogenes	0.0 ± 0.0	15.0 ± 0.0
Acinetobacter baumannii	0.0 ± 0.0	12.4 ± 0.84
Escherichia coli	0.0 ± 0.0	11.2 ± 0.9
Klebsiella pneumonia	0.0 ± 0.0	15.2 ± 0.84
Proteus mirabilis	0.0 ± 0.0	12.0 ± 0.7
Proteus vulgaris	0.0 ± 0.0	10.3 ± 0.58
Pseudomonas aeruginosa	0.0 ± 0.0	14.3 ± 0.72
Candia albicans	0.0 ± 0.0	12.3 ± 0.52

[a] 0 is no inhibition. *A*: plain curcumin and *B*: plain chitosan. The diameter of the inhibition zone is expressed as mean ± SD (experiment conducted in triplicate), $P < 0.05$ or $P < 0.01$.

Cur-CuO NPs exert their effect through their antimicrobial property by the generation of reactive oxygen species (ROS) primarily, damage to the membrane, inhibition of DNA replication, and inhibition of the efflux pump mechanism of bacteria. The as-generated ROS, such as hydroxyl radicals ($OH^{\bullet}$), superoxide anions ($O_2^{\bullet}$), and hydrogen peroxide (H_2O_2), induce oxidative stress, which leads to lipid peroxidation, protein oxidation, and DNA damage.[118] Additionally, membrane permeation is heightened by curcumin due to its polyphenolic nature, which alters the permeability of bacterial membranes and leads to intracellular leakage.[119] Cur-CuO NPs bind with nucleic acid and transcriptional enzymes within the bacterial cells and hinder DNA replication, suppressing protein synthesis together with bacterial growth.[120] Furthermore, curcumin was found to suppress bacterial efflux pumps, which are major contributors to antibiotic resistance, thus adding to the general antimicrobial effect of Cur-CuO NPs, especially against multidrug-resistant (MDR) strains.[121]

CS-CuO NPs utilize electrostatic interactions, ROS-stimulated oxidative damage, and induce metabolic impairment to exert their antimicrobial activity. The effectiveness of the nanocomposite is due to the following processes: firstly, the electrostatic interaction between the positively charged amino ($-NH_3^+$) functional groups in chitosan and the negatively charged bacterial cell membrane lead to the destabilization of the cell membrane, thereby allowing increased permeability and leakage of the vital intracellular components.[122,123] Similar to Cur-CuO NPs, CS-CuO NPs also yield ROS, which in turn causes oxidative damage to bacterial lipids, proteins, and DNA, thus leading to cell dysfunction and death. Contiguously, CS-CuO NPs also interact with bacterial nutrient uptake and the metabolic procedures that lead to ion exchange and energy generation disorders, the occurrence of which negatively affects the bacterial cell life cycle.[34,124] The entry of chitosan in bacterial cells further inhibits the DNA replication and transcription process, and therefore no proteins are produced, preventing their growth. The combinatorial effect of the mechanisms makes CS-CuO NPs highly effective against various bacterial pathogens.[125,126]

Both Cur-CuO and CS-CuO NPs exhibit strong antimicrobial effects due to their unique but partly similar modes of action. Cur-CuO NPs make use of the bioactive properties of curcumin to inhibit efflux pumps and bring about oxidative stress, while CS-CuO NPs work mainly by the destabilization of the electrostatic membrane and metabolic disruption.

3.9. Antimicrobial mechanism based on generation of ROS in bacterial cell

Fig. 11 and Table 10 present the effects of Cur-capped and CS-capped CuO nanoparticles exposure to *S. aureus* and *K. pneumoniae* as models for Gram-positive and Gram-negative bacterial isolates, respectively, compared to the control. The CS-capped CuO NPs produced lower levels of ROS in bacterial cells than Cur-capped CuO NPs. Also, *S. aureus* Gram-positive bacterial isolates were more susceptible to antibacterial based on the induction of ROS than *K. pneumoniae* Gram-negative bacterial isolates using both Cur-capped and CS-capped CuO NPs, which may be due to the difference in the cell wall

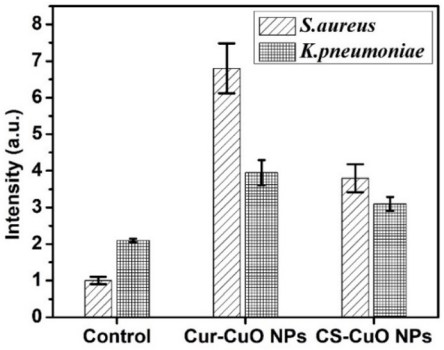

Fig. 11 Antibacterial activity mechanism of Cur-CuO NPs and CS-CuO NPs against *S. aureus* (Gram-positive) and *K. pneumoniae* (Gram-negative).

structure of these two classes and agrees with earlier reports.[127,128] Reactive oxygen species (ROS)-induced oxidative stress plays a critical role in the antibacterial action of copper. ROS are oxygen-containing derivatives that are made up of highly unstable oxygen radicals such as superoxide ($O_2^{\bullet}$), hydroxyl ($OH^{\bullet}$), hydrogen peroxide (H_2O_2), and singlet oxygen (O_2). The atomic or molecular orbitals of ROS contain one or more unpaired electrons, making them very reactive. In this regard, Cu^{2+} ions can cause oxidative damage to the unsaturated fatty acids of the phospholipids in the bacterial cell membrane by producing extracellular ROS, whereas OH can drive the non-enzymatic peroxidation of unsaturated double bonds of fatty acids, triggering a series of reactions and causing extensive changes in the structure of the phospholipid bilayer. This destroys the biophysical properties of the membrane, eventually leading to membrane loss.[128,129]

3.10. Determination of minimum inhibitory concentration (MIC)

The minimum inhibitory concentration (MIC) evaluation for the Cur-CuO NPs and CS-CuO NPs was carried out as shown in Table 11. Results revealed that all the MIC values observed in the case of CS-CuO NPs were lower than those surveyed in Cur-CuO NPs among the investigated microorganisms, where the lowest MIC recorded for Cur-CuO NPs was 14.5 μg mL^{-1} against *Enterococcus faecalis*, while it was 3.9 μg mL^{-1} for CS-CuO NPs against *Streptococcus pyogenes* and *Proteus vulgaris*. The MIC of Cur-CuO was 31.2 μg mL^{-1} for *Staphylococcus aureus* (MSSA) and *Escherichia coli*, whereas it was in the range of 14.5 to 15.6 μg mL^{-1} against the other investigated bacteria and fungi.[130] Alternatively, the MIC of CS-CuO was 4.3 μg mL^{-1} for both *Staphylococcus aureus* (MSSA) and (MRSA) and 4.5, 5.1, 7 and 8.6 μg mL^{-1} for *Enterococcus faecalis*, *Klebsiella pneumonia*, *Proteus mirabilis*, and *Acinetobacter baumannii*, respectively.

Our findings demonstrated that the MIC of CS-CuO NPs against *Acinetobacter baumannii* was 8.6 μg mL^{-1}, which is lower than that reported by Sarfraz and co-workers,[43] stating that the MIC value for CS-CuO was 62.5 μg mL^{-1}. In addition, the MIC (*i.e.*, 14 to 31 μg mL^{-1}) in the current study is lower than the MIC obtained by Sathiyavimal *et al.* (*i.e.*, 25 to 100 μg mL^{-1}).[37]

Table 10 ROS generation by Cur-CuO NPs and CS-CuO NPs against *S. aureus* and *K. pneumoniae*

Bacterial species	Control	Cur-CuO NPs	Cs–CuO NPs
+ve Gram bacteria			
S. aureus	1.0 ± 0.0	6.8 ± 0.66	3.95 ± 0.6
−ve Gram bacteria			
K. pneumoniae	2.1 ± 0.0	3.8 ± 0.55	3.1 ± 0.55

Table 11 MIC values for Cur-CuO NPs and CS-CuO NPs

	Minimum inhibition concentration (μg mL^{-1})	
Microorganism	Cur-CuO NPs	CS-CuO NPs
Staphylococcus aureus (MSSA)	31.2 ± 0.0	4.3 ± 1.2
Staphylococcus aureus (MRSA)	15.2 ± 1.8	4.3 ± 1.4
Enterococcus faecalis	14.5 ± 2.9	4.5 ± 1.5
Streptococcus pyogenes	15.6 ± 0.0	3.9 ± 0.0
Acinetobacter baumannii	14.8 ± 2.4	8.6 ± 2.4
Escherichia coli	31.2 ± 0.0	15.6 ± 0.0
Klebsiella pneumonia	15.1 ± 1.9	5.1 ± 1.8
Proteus mirabilis	15.6 ± 0.0	7.0 ± 1.7
Proteus vulgaris	15.6 ± 0.0	3.9 ± 0.0
Pseudomonas aeruginosa	14.6 ± 2.7	5.2 ± 1.9
Candia albicans	15.6 ± 0.0	5.0 ± 1.9

Also, Jayaramudu *et al.* explored the antibacterial activity against Gram-positive and Gram-negative bacterial isolates with a concertation of 1 mg mL^{-1}, which is also higher than that used in the current study.[113]

3.11. Biocompatibility based on MTT assay

In the biocompatibility assays, WI38 cells, as an *in vitro* test model of a normal cell line, were exposed to both Cur-CuO and CS-CuO NPs, respectively, to determine their (see Fig. 12 and Table 12). In this study, various concentrations of 1.56, 3.125, 6.25, 12.5, 25, 50 and 100 μg mL^{-1} of Cur-CuO NPs, CS-CuO NPs, plain curcumin, plain chitosan, and DOX respectively, were subjected to MTT screening colorimetric assay at a 48 h interval, as shown in Fig. 12. Our results, as presented in Table 12, showed that Cur-CuO NPs have an IC_{50} dose of 74.17 μg mL^{-1}, which is higher than that of CS-CuO NPs with IC_{50} of 41.01 μg mL^{-1}. In addition, Cur-CuO NPs were found to be safer than both plain chitosan (IC_{50} of ∼65.8 μg mL^{-1}) and DOX (IC_{50} of ∼6.72 μg mL^{-1}). Moreover, the lowest cytotoxic effect was observed for plain curcumin with an IC_{50} of 92.17 μg mL^{-1} (see Table 12). In the case of Cur-CuO NPs, the highest dose could kill about 55% of cells, whereas when applied at low concentrations of 1.56, 3.125 and 6.25 μg mL^{-1}, they only killed 0 and 1.8%, respectively, of cells after 48 h of cell exposure (Fig. 12). Treatment of cells with the highest concentration of 100 μg mL^{-1} CS-CuO NPs killed about 68% of the cells, whereas treatment of cells with low concentrations of 1.56, 3.125 and 6.25 μg mL^{-1} killed about 0 and 6.6% of the cells after 48 h of exposure (Fig. 12).

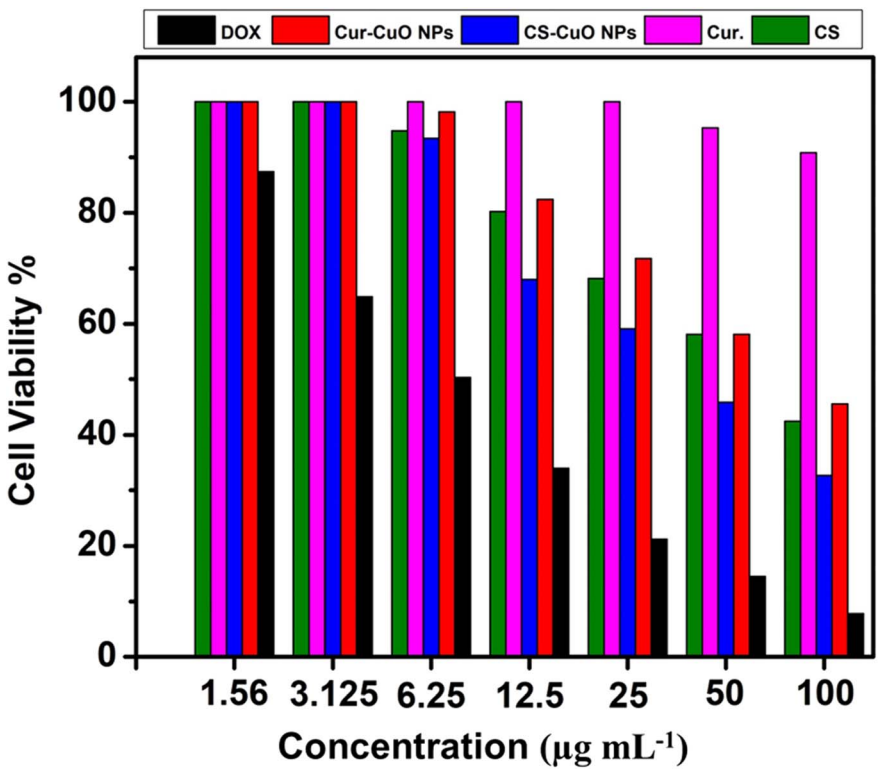

Fig. 12 Biocompatibility assay of Cur-CuO NPs, CS-CuO NPs, plain curcumin, plain chitosan and DOX at different levels of exposure doses.

3.11. Comparison with other antimicrobial agents and traditional antibiotics

In this work, the effectiveness of Cur-CuO and CS-CuO nanoparticles was compared to our previous studies on the Cur-Ag and Cur-ZnO materials and traditional drugs such as ciprofloxacin, amoxicillin, gentamicin, and vancomycin.[4] The outcomes revealed that Cur-Ag NPs possess the maximum antibacterial function, which are superior to the traditional antibiotics, particularly MRSA, *Pseudomonas aeruginosa*, and *Candida albicans*. Furthermore, CS-CuO NPs were found to demonstrate significant antibacterial activity and the results showed that they were as effective as gentamicin and vancomycin making them a suitable alternative. Although the traditional antibiotics, especially ciprofloxacin, have lower minimum inhibitory concentration (MIC) values, and thus they are proven to be more potent, the nanoparticles still remained quite efficient, especially against the drug-resistant bacterial strains. In comparison with other nanoparticles, Cur-Ag NPs had the largest zones of inhibition and lowest MIC values at every stage, whereas CS-CuO NPs were almost compatible showing their antimicrobial property, as shown in Table 13.

In contrast, Cur-CuO and CS-CuO NPs showed higher biocompatibility and safety than the Cur-Ag NPs and Cur-ZnO NPs mentioned in our previous study.[4] Cur-CuO NPs and CS-CuO NPs have an IC_{50} dose of 74 and 41 μg mL^{-1}, respectively, which is higher than the recorded IC_{50} of Cur-Ag and Cur-ZnO NPs of 30 μg mL^{-1} mentioned in our previous work.[4]

Table 12 Calculated IC_{50} of Cur-CuO and CS-CuO NPs against WI38 cell line compared with DOX, plain curcumin and chitosan as controls[a,b]

No.	Sample	Lethal cytotoxic dose (IC_{50}, μg mL^{-1})
Cont	DOX	6.72 ± 0.5
1	Cur-CuO NPs	74.17 ± 3.7
2	CS-CuO NPs	41.01 ± 2.2
3	Plain curcumin	92.17 ± 4.2
4	Plain chitosan	65.80 ± 3.1

[a] IC_{50} (ppm): 1–10 (very strong). 11–20 (strong). 21–50 (moderate). 51–100 (weak) and above 100 (non-cytotoxic). [b] DOX: doxorubicin data were measured after 48 h. Means a significant difference ($P < 0.05$) compared to the control. Mean ± SD (experiment conducted in triplicate).

3.12. Potential applications in healthcare and antimicrobial strategies

These nanoparticles can be combined with another drug to make new antimicrobial compositions. In a treatment plan implementation, glass substrates and glasses are effective in the prevention of biofilm formation and device-associated infections to be used as coatings of medical devices, such as catheters, implants, and ventilators. In addition, they can be considered good alternatives to some hospital equipment such as filtration membranes, tubing, prosthesis, artificial lung devices, resistivity measurement, manufacturing processes, and air disinfection systems.

Cur-CuO and CS-CuO NPs have been proven as promising materials that have the potential to replace the traditional antibiotics of the past. This is because of their broad-spectrum antimicrobial activity, which targets the whole spectrum of microorganisms. Furthermore, although the biocompatible chitosan coating ensures that the development of resistance is prevented, it is also beneficial. Thus, if the most efficient and effective building-related technologies are implemented, considerable energy reduction can be achieved.

Cur-CuO and CS-CuO nanoparticles are microorganisms that have broad variability to different drugs, which range from those which can kill microorganisms to other drugs with an inhibitory effect on growth. The structural and physical properties of these CuO nanomaterials include hardness, brittleness, and uniaxial orientation of their crystals.

Their main function is oxidative stress induction and bacterial membrane disruption, which make it hard for pathogens to develop resistance, thus overcoming this big issue when trying to fight infections. Another potential use is in inhalable aerosol formulations for respiratory infections, especially in ICUs where there are many cases of pneumonia that are resistant to antibiotics, and thus a very concerning development.

Table 13 Comparison of antimicrobial activity (zone of inhibition in mm and MIC in μg mL^{-1})[a]

Microorganism	Cur-CuO NPs	CS-CuO NPs	Cur-Ag NPs	Cur-ZnO NPs	Ciprofloxacin	Amoxicillin	Gentamicin	Vancomycin
Staphylococcus aureus (MSSA)	14.5/5.0	20.5/3.2	21.2/2.5	18.4/3.8	24.1/1.2	15.6/8.0	20.3/2.0	18.2/3.5
Staphylococcus aureus (MRSA)	16.6/4.2	19.1/3.0	22.5/2.1	19.2/3.5	21.3/1.5	12.4/9.3	18.6/2.3	16.8/4.0
Enterococcus faecalis	15.1/6.0	24.4/3.5	20.8/3.0	18.9/4.0	23.0/2.0	14.2/10.5	19.0/3.5	21.6/3.8
Streptococcus pyogenes	16.5/5.8	19.0/3.3	21.3/2.8	19.0/3.9	25.3/1.8	15.8/7.8	20.5/2.8	18.7/3.6
Acinetobacter baumannii	15.4/6.5	16.3/4.0	18.9/3.5	16.2/4.2	20.4/2.3	11.7/12.0	16.5/4.0	14.3/4.8
Escherichia coli	14.3/6.8	16.2/4.2	20.0/3.2	17.4/4.5	23.5/1.7	13.5/11.2	19.8/3.3	15.9/4.6
Klebsiella pneumoniae	15.0/6.3	19.5/4.0	20.6/3.3	18.1/4.4	22.1/2.0	14.0/10.8	18.9/3.4	16.5/4.2
Proteus mirabilis	16.0/6.1	18.4/3.8	19.5/3.4	17.5/4.2	21.7/2.1	12.9/9.7	17.6/3.6	15.8/4.0
Proteus vulgaris	17.3/5.9	19.3/3.6	21.8/2.9	19.0/3.8	22.5/1.9	14.8/8.9	19.2/3.1	16.4/3.7
Pseudomonas aeruginosa	16.4/6.7	21.4/4.5	22.1/3.8	18.7/4.6	23.0/2.5	13.9/10.2	20.1/3.7	16.9/4.5
Candida albicans	16.4/6.4	20.1/4.1	22.0/3.0	19.5/4.3	21.0/2.0	12.7/11.0	18.5/3.5	14.7/5.0

[a] The values are represented as zone of inhibition (mm)/MIC (μg mL^{-1}).

4. Conclusion

In the present study, curcumin- and chitosan-capped copper oxide nanoparticles (Cur-CuO and CS-CuO NPs) were successfully green synthesized in the presence of an ethanolic extract of *Curcuma longa* Linns (synonym; *Curcuma domestica* Valeton, Zingiberaceae) and 1% aqueous solution of acetic acid, respectively. The average particle sizes with spherical shape were 25 ± 10 (Cur-CuO NPs) and 10 ± 5 nm (CS-CuO NPs). In addition, their antimicrobial activity was investigated against several multi-drug resistance (MDR) bacterial and fungal isolates. The tested microorganisms were clinically isolated from patients suffering from different infections. Identification and frequency determination for these microorganisms revealed *Klebsiella pneumoniae* as the most frequent (25.8% of total isolated strains), followed by *Staphylococcus aureus* (MRSA) (14.8% of total isolated strains). *Streptococcus pyogenes* had the lowest representation, with only 1.6% of the strains. *Candida albicans* was the only recorded fungi, comprising 5.5% of the isolated strains. In addition, the isolated microorganisms showed complete resistance to about 14 antibiotics from 21 tested antibiotics. Cur-CuO and CS-CuO NPs were effective against all the clinically isolated microorganisms, even when using the lowest investigated concentration. In addition, the results for both Cur-CuO NPs and CS-CuO NPs revealed that overall, the minimum inhibitory concentration was lower for the chitosan-capped copper oxide nanoparticles compared with the curcumin-capped copper oxide nanoparticles, with values of 3.9 μg mL^{-1} to 15.6 μg mL^{-1} for CS-CuO NPs, while 14.5 to 31.2 μg mL^{-1} for Cur-CuO NPs. The antimicrobial activity for plain curcumin and plain chitosan was investigated, reflecting that plain curcumin did not show any antimicrobial activity; conversely, plain chitosan showed strong antimicrobial activity, giving zones of inhibition ranging in size from 10.3 to 15.2 mm against *Proteus vulgaris* and *Klebsiella pneumonia*, respectively. However, after capping CuO with curcumin, the complex has strong antimicrobial activity, which could be due to the binding of the curcumin to the bacterial or fungal cell membrane, thus facilitating the penetration of CuO into the interior of the cells, leading to the formation of ROS and DNA damage.[131,132] The remarkable efficacy of the curcumin- and chitosan-capped copper oxide nanoparticles in effectively combating highly resistant multi-drug pathogens highlights their promising potential for future applications. Finally, the biocompatibility assay showed that Cur-CuO NPs have an IC_{50} dose of 74.17 μg mL^{-1}, which is higher than that of CS-CuO NPs with an IC_{50} of 41.01 μg mL^{-1}. In addition, Cur-CuO NPs exhibited higher safety than both plain chitosan (IC_{50} of ~65.8 μg mL^{-1}) and DOX (IC_{50} of ~6.72 μg mL^{-1}). The obtained results show that Cur-CuO NPs are safer to use as an antimicrobial agent compared to CS-CuO NPs. However, both Cur-CuO and CS-CuO NPs could be safely used at low concentrations of 6.25 to 12.5 μg mL^{-1}. Our findings highlight the applicability of using Cur-CuO NPs and CS-CuO NPs and how the capping procedure could affect antimicrobial activity.

Ethical approval

This study was performed in strict accordance with the GOTHI guidelines ethics regulations issued by the Minister of Health & Population Cairo, Egypt: no. 238/2003, Articles 52-6121, approved by the medical research ethics committee. In addition, the approval for performing this study has been registered under No IME 00069 in 2022.

Data availability

The data supporting this article have been included as part of the ESI.†

Author contributions

Noura El-Kattan; conceptualization, performed all the microbiological studies and contributed to manuscript writing. Mostafa Ahmed Ibrahim and Ahmed Sadek Mansour; synthesis of nanomaterials, performed TEM imaging and their analysis & discussion. Ahmed Nabile Emam (Corresponding author) performed characterization experiments, including UV-vis optical absorption spectroscopy, FTIR, dynamic light scattering (DLS), EDX elemental analysis, XRD and zeta potential. In addition, data analysis, writing/formulating, revision, and submission of the manuscript. Khaled Metwally: contributed to cytotoxicity assay, the discussion on the microbiological part and in writing of the manuscript. Fady Sayed Youssef: performed the gas chromatography-mass spectrometry (GC-MS) on the ethanolic extract of *Curcuma longa* Linn (turmeric) powder *vs.* the pure curcumin. Nourelhuda Ahmed; contributed to cytotoxicity assay. Documentation of patient's data and collection of the clinical samples, including blood, sputum, wound, and urine, from patients admitted to the intensive care unit (ICU) in El-Sahel Teaching Hospital, the general organization for teaching hospitals and institutes (GOTHI), Cairo, Egypt.

Conflicts of interest

The authors have no relevant financial or non-financial interests to disclose.

Acknowledgements

The authors are grateful to Prof. Ashraf Bakry Abd El-Razik and NanoFab Technology for funding the Chemicals used in the fabrication of nanomaterials. In addition, funding the TEM imaging investigation that was included and used in this study.

Notes and references

1 E. L. Tsalik, Y. Li, L. L. Hudson, V. H. Chu, T. Himmel, A. T. Limkakeng, J. N. Katz, S. W. Glickman, M. T. McClain and K. E. Welty-Wolf, *Ann. Am. Thorac. Soc.*, 2016, **13**, 401–413.
2 T. Gottlieb and G. R. Nimmo, *Med. J. Aust.*, 2011, **194**, 281–283.

3 M. S. Usman, M. E. E. Zowalaty, K. Shameli, N. Zainuddin, M. Salama and N. A. Ibrahim, *Int. J. Nanomed.*, 2013, 4467–4479.
4 N. El-Kattan, A. N. Emam, A. S. Mansour, M. A. Ibrahim, A. B. Abd El-Razik, K. A. Allam, N. Y. Riad and S. A. Ibrahim, *RSC Adv.*, 2022, **12**, 18022–18038.
5 A. Rahman, A. Ismail, D. Jumbianti, S. Magdalena and H. Sudrajat, *Indones. J. Chem.*, 2009, **9**, 355–360.
6 M. Ahamed, H. A. Alhadlaq, M. M. Khan, P. Karuppiah and N. A. Al-Dhabi, *J. Nanomater.*, 2014, **2014**, 17.
7 K. Gopalakrishnan, C. Ramesh, V. Ragunathan and M. Thamilselvan, *Digest J. Nanomater. Biostruct.*, 2012, **7**, 833–839.
8 S. Jagadeeshan and R. Parsanathan, *Advanced Nanostructured Materials for Environmental Remediation*, 2019, pp. 59–90.
9 V. Stanić and S. B. Tanasković, in *Nanotoxicity*, Elsevier, 2020, pp. 241–274.
10 L. Bruslind, *Microbiology*, Open Oregon Stat, Corvallis, OR, USA, 2017.
11 E. Sánchez-López, D. Gomes, G. Esteruelas, L. Bonilla, A. L. Lopez-Machado, R. Galindo, A. Cano, M. Espina, M. Ettcheto and A. Camins, *Nanomaterials*, 2020, **10**, 292.
12 M. C. Stensberg, Q. Wei, E. S. McLamore, D. M. Porterfield, A. Wei and M. S. Sepúlveda, *Nanomedicine*, 2011, **6**, 879–898.
13 S. Aruna, N. Vasugi Raaja and S. Sathiesh Kumar, *Int. J. Innov. Res. Sci. Eng. Technol.*, 2016, **5**, 2112–2119.
14 I. Subhankari and P. Nayak, *World J. Nanosci. Nanotechnol.*, 2013, **2**, 10–13.
15 A. M. Eid, A. Fouda, S. E.-D. Hassan, M. F. Hamza, N. K. Alharbi, A. Elkelish, A. Alharthi and W. M. Salem, *Catalysts*, 2023, **13**, 348.
16 U. T. Khatoon, A. Velidandi and G. N. Rao, *Inorg. Chem. Commun.*, 2023, 110372.
17 G. Ungur and J. Hruza, *Fibers Polym.*, 2015, **16**, 621–628.
18 S. P. Selvaraj, *Mater. Today: Proc.*, 2022, **50**, 2865–2868.
19 N. Y. Lee, W. C. Ko and P. R. Hsueh, *Front. Pharmacol*, 2019, **10**, 1153.
20 O. O. Adeniji, N. Nontongana, J. C. Okoh and A. I. Okoh, *Int. J. Mol. Sci.*, 2022, **23**, 15038.
21 G. Waktole and B. Chala, *J. Biomater. Nanobiotechnol.*, 2023, **14**, 1–22.
22 A. Goel, A. B. Kunnumakkara and B. B. Aggarwal, *Biochem. Pharmacol.*, 2008, **75**, 787–809.
23 S. J. Hewlings and D. S. Kalman, *Foods*, 2017, **6**, 92.
24 M. Karandish, H. Mozaffari-Khosravi, S. M. Mohammadi, M. Azhdari and B. Cheraghian, *Trials*, 2020, **21**, 1–11.
25 I. Brouet and H. Ohshima, *Biochem. Biophys. Res. Commun.*, 1995, **206**, 533–540.
26 S. Cikrikci, E. Mozioglu and H. Yilmaz, *Rec. Nat. Prod.*, 2008, **2**, 19.
27 P. Anand, A. B. Kunnumakkara, R. A. Newman and B. B. Aggarwal, *Mol. Pharmaceutics*, 2007, **4**, 807–818.
28 H. Elabd, H. H. Mahboub, S. M. R. Salem, A. M. Abdelwahab, K. M. Alwutayd, M. Shaalan, S. H. Ismail, A. M. Abdelfattah, A. Khalid, A. T. Mansour, H. S. Hamed and H. Youssuf, *Fishes*, 2023, **8**, 333.
29 J. Sharifi-Rad, Y. El Rayess, A. Abi Rizk, C. Sadaka, R. Zgheib, W. Zam, S. Sestito, S. Rapposelli, K. Neffe-Skocińska and D. Zielińska, *Front. Pharmacol.*, 2020, **11**(2020), 550909.
30 M. Kumari and D. K. Nanda, *Burns*, 2022, **49**(5), 1003–1016.
31 D. Zheng, C. Huang, H. Huang, Y. Zhao, M. R. U. Khan, H. Zhao and L. Huang, *Chem. Biodiversity*, 2020, **17**, e2000171.
32 A. Guarnieri, M. Triunfo, C. Scieuzo, D. Ianniciello, E. Tafi, T. Hahn, S. Zibek, R. Salvia, A. De Bonis and P. Falabella, *Sci. Rep.*, 2022, **12**, 8084.
33 S. K. Shukla, A. K. Mishra, O. A. Arotiba and B. B. Mamba, *Int. J. Biol. Macromol.*, 2013, **59**, 46–58.
34 D. Yan, Y. Li, Y. Liu, N. Li, X. Zhang and C. Yan, *Molecules*, 2021, **26**, 7136.
35 C.-L. Ke, F.-S. Deng, C.-Y. Chuang and C.-H. Lin, *Polymers*, 2021, **13**, 904.
36 D. Bharathi, R. Ranjithkumar, B. Chandarshekar and V. Bhuvaneshwari, *Int. J. Biol. Macromol.*, 2019, **141**, 476–483.
37 S. Sathiyavimal, S. Vasantharaj, T. Kaliannan and A. Pugazhendhi, *Carbohydr. Polym.*, 2020, **241**, 116243.
38 P. S. Umoren, D. Kavaz, A. Nzila, S. S. Sankaran and S. A. Umoren, *Polymers*, 2022, **14**, 1832.
39 S. B. Ahmed, H. I. Mohamed, A. M. Al-Subaie, A. I. Al-Ohali and N. M. Mahmoud, *Sci. Rep.*, 2021, **11**, 9540.
40 A. R. Maheo, *Results in Surf. and Interf.*, 2022, **6**, 100048.
41 S. Sathiyavimal, S. Vasantharaj, T. Kaliannan, H. A. Garalleh, M. Garaleh, K. Brindhadevi, N. T. L. Chi, A. Sharma and A. Pugazhendhi, *Environ. Res.*, 2023, **218**, 114986.
42 M. H. Sarfraz, S. Muzammil, S. Hayat, M. Khurshid and A. H. Sayyid, *Int. J. Biol. Macromol.*, 2023, **242**, 124954.
43 M. H. Sarfraz, M. Zubair, B. Aslam, A. Ashraf, M. H. Siddique, S. Hayat, J. N. Cruz, S. Muzammil, M. Khurshid and M. F. Sarfraz, *Front. Microbiol.*, 2023, **14**, 1188743.
44 Y. Haldorai and J.-J. Shim, *Int. J. Photoenergy*, 2013, **2013**(1), 245646.
45 K. Varaprasad, M. López, D. Núñez, T. Jayaramudu, E. R. Sadiku, C. Karthikeyan and P. Oyarzúnc, *J. Mol. Liq.*, 2020, **300**, 112353.
46 S. Faisal, N. S. Al-Radadi, H. Jan Abdullah, S. A. Shah, S. Shah, M. Rizwan, Z. Afsheen, Z. Hussain, M. N. Uddin, M. Idrees and N. Bibi, *Coatings*, 2021, **11**, 849.
47 N. Rabiee, M. Bagherzadeh, M. Kiani, A. M. Ghadiri, F. Etessamifar, A. H. Jaberizadeh and A. Shakeri, *Int. J. Nanomed.*, 2020, **15**, 3983–3999.
48 A. M. Beyene, M. Moniruzzaman, A. Karthikeyan and T. Min, *Nanomaterials*, 2021, **11**(2), 460.
49 A. R. Maheo, B. S. M. Vithiya, T. A. A. Prasad, P. Tamizhdurai and V. Mangesh, *Arabian J. Chem.*, 2022, **15**, 103661.
50 W. WC, *Koneman's Color Atlas and Textbook of Diagnostic Microbiology*, 2006, pp. 67–110.

51 B. A. Forbes, D. F. Sahm and A. S. Weissfeld, *Bailey & Scott's Diagnostic Microbiology*, Mosby, St. Louis, 12th edn, 2007, pp. 187–214.
52 P. A. Wayne, *Clinical and laboratory standards institute: performance standards for antimicrobial susceptibility testing: informational supplement, M100*, Clinical and Laboratory Standards Institute (CLSI), 2018.
53 A.-P. Magiorakos, A. Srinivasan, R. B. Carey, Y. Carmeli, M. Falagas, C. Giske, S. Harbarth, J. Hindler, G. Kahlmeter and B. Olsson-Liljequist, *Clin. Microbiol. Infect.*, 2012, **18**, 268–281.
54 F. R. Cockerill, M. Wikler, K. Bush, M. Dudley, G. Eliopoulos and D. Hardy, *Performance Standards for Antimicrobial Susceptibility Testing: Twenty-Second Informational Supplement*, 2012.
55 C. Negrei, A. Hudita, O. Ginghina, B. Galateanu, S. N. Voicu, M. Stan, M. Costache, C. Fenga, N. Drakoulis and A. M. Tsatsakis, *Front. Pharmacol.*, 2016, **7**, 172.
56 N. J. Schmidt, *Enteroviruses and Reoviruses*, 1995, pp. 513–579.
57 A. Emam, S. Loutfy, A. Mostafa, H. Awad and M. Mohamed, *RSC Adv.*, 2017, 7(38), 23502–23514.
58 T. Mosmann, *J. Immunol. Methods*, 1983, **65**, 55–63.
59 F. Denizot and R. Lang, *J. Immunol. Methods*, 1986, **89**, 271–277.
60 F. Zsila, Z. Bikádi and M. Simonyi, *Org. Biomol. Chem.*, 2004, **2**, 2902–2910.
61 C. F. Chignell, P. Bilskj, K. J. Reszka, A. G. Motten, R. H. Sik and T. A. Dahl, *Photochem. Photobiol.*, 1994, **59**, 295–302.
62 G. Stati, F. Rossi, T. Trakoolwilaiwan, L. D. Tung, S. Mourdikoudis, N. T. K. Thanh and R. Di Pietro, *Molecules*, 2022, **27**, 282.
63 D. Setyaningsih, Y. B. Murti, A. Fudholi, W. L. Hinrichs, R. Mudjahid, S. Martono and T. Hertiani, *Indones. J. Pharm. Sci.*, 2017, **14**, 147–157.
64 S. Kamble and R. Dahake Pavan, *Int. J. Contemp. Res. Multidiscipl.*, 2015, **3**, 90–96.
65 I. I. Anekwe, C. I. Chikwendu, E. S. Amadi, N. U. Nwogwugwu and F. C. Ihenetu, *Int. J. Biol. Chem. Sci.*, 2023, **17**, 1199–1207.
66 N. K. M. Altir, A. M. A. Ali, A.-R. Z. Gaafar, A. A. Qahtan, E. M. Abdel-Salam, A. Alshameri, M. S. Hodhod and B. Almunqedhi, *Open Chem.*, 2021, **19**, 945–952.
67 J. O. Momoh, A. A. Manuwa and Y. O. Bankole, *J. Adv. Microbiol.*, 2022, **22**, 116–131.
68 Y. Zheng, C. Pan, Z. Zhang, W. Luo, X. Liang, Y. Shi, L. Liang, X. Zheng, L. Zhang and Z. Du, *Microchem. J.*, 2020, **154**, 104608.
69 A. F. Guimarães, A. C. A. Vinhas, A. F. Gomes, L. H. Souza and P. B. Krepsky, *Quim. Nova*, 2020, **43**, 909–913.
70 G. B. Avanço, F. D. Ferreira, N. S. Bomfim, R. M. Peralta, T. Brugnari, C. A. Mallmann, B. A. de Abreu Filho, J. M. G. Mikcha and M. Machinski Jr, *Food Control*, 2017, **73**, 806–813.
71 N. Motohashi, C. Yamagami, H. Tokuda, T. Konoshima, Y. Okuda, M. Okuda, T. Mukainaka, H. Nishino and Y. Saito, *Cancer Lett.*, 1998, **134**, 37–42.
72 A. Gupta, S. Mahajan and R. Sharma, *Biotechnol. Rep.*, 2015, **6**, 51–55.
73 I. I. Anekwe, C. I. Chikwendu, E. S. Amadi, N. U. Nwogwugwu and F. C. Ihenetu, *Int. J. Biol. Chem. Sci.*, 2023, **17**(3), 1199–1207.
74 B. H. Kebede, S. F. Forsido, Y. B. Tola and T. Astatkie, *Heliyon*, 2021, **7**(2), e06239.
75 H. Van Nong, L. X. Hung, P. N. Thang, V. D. Chinh, L. V. Vu, P. T. Dung, T. Van Trung and P. T. Nga, *SpringerPlus*, 2016, **5**, 1147.
76 S. S. Hettiarachchi, S. P. Dunuweera, A. N. Dunuweera and R. G. Rajapakse, *ACS Omega*, 2021, **6**, 8246–8252.
77 A. Putri, T. Octavianty, N. Wahyudi and A. Safitri, *J. Phys.: Conf. Ser.*, 2019, **1374**(1), 012027.
78 R. S. Nunavath, K. C. Bhadram and K. Nagappan, *J. Pharm. Biomed. Anal.*, 2023, **235**, 115614.
79 O. N. Gordon and C. Schneider, *Trends Mol. Med.*, 2012, **18**, 361–364.
80 A. Rohman, D. Ramadhani and A. Nugroho, *Res. J. Med. Plant*, 2015, **9**, 179–186.
81 M. Qasem, R. El Kurdi and D. Patra, *ChemistrySelect*, 2020, **5**, 1694–1704.
82 N. E. Safie, N. A. Ludin, M. S. Su'ait, N. H. Hamid, S. Sepeai, M. A. Ibrahim and M. A. M. Teridi, *Malay. J. Anal. Sci.*, 2015, **19**, 1243–1249.
83 S. Bhattacharjee, *J. Controlled Release*, 2016, **235**, 337–351.
84 D. Patra and R. El Kurdi, *Green Chem. Lett. Rev.*, 2021, **14**, 474–487.
85 M. Danaei, M. Dehghankhold, S. Ataei, F. Hasanzadeh Davarani, R. Javanmard, A. Dokhani, S. Khorasani and M. Mozafari, *Pharmaceutics*, 2018, **10**, 57.
86 S. Dasgupta, S. Das, N. S. Chawan and A. Hazra, *Indian J. Crit. Care Med.*, 2015, **19**, 14.
87 S. Stefani, D. R. Chung, J. A. Lindsay, A. W. Friedrich, A. M. Kearns, H. Westh and F. M. MacKenzie, *Int. J. Antimicrob. Agents*, 2012, **39**, 273–282.
88 S. Y. Tong, J. S. Davis, E. Eichenberger, T. L. Holland and V. G. Fowler Jr, *Clin. Microbiol. Rev.*, 2015, **28**, 603–661.
89 J. A. Lindsay, *Int. J. Med. Microbiol.*, 2014, **304**, 103–109.
90 B. Mlynarczyk-Bonikowska, C. Kowalewski, A. Krolak-Ulinska and W. Marusza, *Int. J. Mol. Sci.*, 2022, **23**, 8088.
91 G. Sakoulas, A. S. Bayer, J. Pogliano, B. T. Tsuji, S.-J. Yang, N. N. Mishra, V. Nizet, M. R. Yeaman and P. A. Moise, *Antimicrob. Agents Chemother.*, 2012, **56**, 838–844.
92 J. Top, R. Willems and M. Bonten, *FEMS Immunol. Med. Microbiol.*, 2008, **52**, 297–308.
93 A. R. Freitas, C. Novais, A. P. Tedim, M. V. Francia, F. Baquero, L. Peixe and T. M. Coque, *PLoS One*, 2013, **8**, e60589.
94 D. Yu, Y. Zheng and Y. Yang, *Infect. Drug Resist.*, 2020, 2323–2327.
95 I. Kyriakidis, E. Vasileiou, Z. D. Pana and A. Tragiannidis, *Pathogens*, 2021, **10**, 373.
96 C.-R. Lee, J. H. Lee, M. Park, K. S. Park, I. K. Bae, Y. B. Kim, C.-J. Cha, B. C. Jeong and S. H. Lee, *Front. Cell. Infect. Microbiol.*, 2017, **7**, 55.

97 Y.-F. Zhou, P. Liu, C.-J. Zhang, X.-P. Liao, J. Sun and Y.-H. Liu, *Front. Microbiol.*, 2020, **10**, 2957.
98 Y. Paitan, *Escherichia coli, a Versatile Pathogen*, 2018, pp. 181–211.
99 G. Granata and N. Petrosillo, *Infect. Dis. Rep.*, 2017, **9**, 7104.
100 M. Bassetti, E. Righi, A. Carnelutti, E. Graziano and A. Russo, *Expert Rev. Anti-Infect. Ther.*, 2018, **16**, 749–761.
101 B. Jana, A. K. Cain, W. T. Doerrler, C. J. Boinett, M. C. Fookes, J. Parkhill and L. Guardabassi, *Sci. Rep.*, 2017, **7**, 42483.
102 S. V. Chakka, N. Thanjavur, S. Lee and S. Kim, *J. Rare Earths*, 2022, **41**(10), 1606–1615.
103 C. Karthikeyan, K. Varaprasad, A. Akbari-Fakhrabadi, A. S. H. Hameed and R. Sadiku, *Carbohydr. Polym.*, 2020, **249**, 116825.
104 N. Jayarambabu, A. Akshaykranth, T. V. Rao, K. V. Rao and R. R. Kumar, *Mater. Lett.*, 2020, **259**, 126813.
105 M. Jayandran, M. M. Haneefa and V. Balasubramanian, *Indian J. Sci. Technol.*, 2016, **9**, 1–9.
106 K. Cheraghipour, B. Ezatpour, L. Masoori, A. Marzban, A. Sepahvand, A. K. Rouzbahani, A. Moridnia, S. Khanizadeh and H. Mahmoudvand, *Curr. Drug Discovery Technol.*, 2021, **18**, 379–390.
107 I. M. El-Nahhal, J. Salem, F. S. Kodeh, A. Elmanama and R. Anbar, *Mater. Chem. Phys.*, 2022, **285**, 126099.
108 J. K. Trigo-Gutierrez, Y. Vega-Chacón, A. B. Soares and E. G. D. O. Mima, *Int. J. Mol. Sci.*, 2021, **22**, 7130.
109 N. P. Rajkumari, P. Roy, S. Siddika, K. Adhikary and P. Goswami, *Mater. Sci. Eng. B.*, 2023, **292**, 116416.
110 C. D. Tran, J. Makuvaza, E. Munson and B. Bennett, *ACS Appl. Mater. Interfaces*, 2017, **9**, 42503–42515.
111 S. Logpriya, V. Bhuvaneshwari, D. Vaidehi, R. SenthilKumar, R. Nithya Malar, B. Pavithra Sheetal, R. Amsaveni and M. Kalaiselvi, *J. Nanostruct. Chem.*, 2018, **8**, 301–309.
112 J. Li and S. Zhuang, *Eur. Polym. J.*, 2020, **138**, 109984.
113 T. Jayaramudu, K. Varaprasad, R. D. Pyarasani, K. K. Reddy, K. D. Kumar, A. Akbari-Fakhrabadi, R. Mangalaraja and J. Amalraj, *Int. J. Biol. Macromol.*, 2019, **128**, 499–508.
114 B. Vishalakshi, B. Umakanth, A. P. Shanbhag, A. Ghatak, N. Sathyanarayanan, M. Madhav, G. G. Krishna and H. Yadla, *3 Biotech*, 2017, **7**, 1–6.
115 N. Zainuddin, I. Ahmad, H. Kargarzadeh and S. Ramli, *Carbohydr. Polym.*, 2017, **163**, 261–269.
116 H. Tan, R. Ma, C. Lin, Z. Liu and T. Tang, *Int. J. Mol. Sci.*, 2013, **14**, 1854–1869.
117 M. Kong, X. G. Chen, K. Xing and H. J. Park, *Int. J. Food Microbiol.*, 2010, **144**, 51–63.
118 Z. Song, Y. Wu, H. Wang and H. Han, *Mater. Sci. Eng. C*, 2019, **99**, 255–263.
119 L. Wang, C. Hu and L. Shao, *Int. J. Nanomed.*, 2017, 1227–1249.
120 C. Gunawan, W. Y. Teoh, C. P. Marquis and R. Amal, *ACS Nano*, 2011, **5**, 7214–7225.
121 S. Zorofchian Moghadamtousi, H. Abdul Kadir, P. Hassandarvish, H. Tajik, S. Abubakar and K. Zandi, *BioMed Res. Int.*, 2014, **2014**(1), 186864.
122 D. Raafat and H. G. Sahl, *Microb. Biotechnol.*, 2009, **2**, 186–201.
123 W. Sajomsang, P. Gonil and S. Tantayanon, *Int. J. Biol. Macromol.*, 2009, **44**, 419–427.
124 G. Kravanja, M. Primožič, Ž. Knez and M. Leitgeb, *Molecules*, 2019, **24**, 1960.
125 J. Vinsova and E. Vavrikova, *Curr. Pharm. Des.*, 2011, **17**, 3596–3607.
126 S. Paul, D. MK and S. Peter, *J. Pharm. Innovation*, 2022, 1–10.
127 G. Applerot, J. Lellouche, A. Lipovsky, Y. Nitzan, R. Lubart, A. Gedanken and E. Banin, *Small*, 2012, **8**, 3326–3337.
128 X. Ma, S. Zhou, X. Xu and Q. Du, *Front. Surg.*, 2022, **9**, 905892.
129 M. Tiwari, K. Narayanan, M. B. Thakar, H. V. Jagani and J. Venkata Rao, *IET Nanobiotechnol.*, 2014, **8**, 230–237.
130 S.-Y. Teow, S. A. Ali and P. J. Pharm, *Sci*, 2015, **28**, 2109–2114.
131 A. A. Targhi, A. Moammeri, E. Jamshidifar, K. Abbaspour, S. Sadeghi, L. Lamakani and I. Akbarzadeh, *Bioorg. Chem.*, 2021, **115**, 105116.
132 P. Bhavyasree and T. Xavier, *Curr. Res. Green Sustainable Chem.*, 2022, **5**, 100249.